





Strain migration during multiphase extension, Stord Basin, northern North Sea rift

Hamed Fazlikhani^{1,2}  | Synne S. Aagotnes^{2,3} | Marte A. Refvem^{2,4} |
James Hamilton-Wright^{5,6} | Rebecca E. Bell⁵ | Haakon Fossen^{7,2} |
Robert L. Gawthorpe²  | Christopher A.-L. Jackson⁵  | Atle Rotevatn² 

¹GeoZentrum Nordbayern, Friedrich-Alexander-Universität (FAU) Erlangen-Nürnberg, Erlangen, Germany

²Department of Earth Science, University of Bergen, Bergen, Norway

³Now at Petrolia NOCO AS, Bergen, Norway

⁴Now at Equinor ASA, Bergen, Norway

⁵Basins Research Group (BRG), Department of Earth Science and Engineering, Imperial College, London, UK

⁶BP Exploration Operating Company Limited, Sunbury-on-Thames, Middlesex, UK

⁷Natural History Collections, University of Bergen, Bergen, Norway

Correspondence

Hamed Fazlikhani, GeoZentrum Nordbayern, Friedrich-Alexander-Universität (FAU) Erlangen-Nürnberg, Erlangen, Germany.
Email: hamed.fazlikhani@gmail.com

Funding information

Norges Forskningsråd, Grant/Award Number: PETROMAKS project 215591

Abstract

In regions experiencing multiple phases of extension, rift-related strain can vary along and across the basin during and between each phase, and the location of maximum extension can differ between the rift phase. Despite having a general understanding of multiphase rift kinematics, it remains unclear why the rift axis migrates between extension episodes. The role pre-existing structures play in influencing fault and basin geometries during later rifting events is also poorly understood. We study the Stord Basin, northern North Sea, a location characterised by strain migration between two rift episodes. To reveal and quantify the rift kinematics, we interpreted a dense grid of 2D seismic reflection profiles, produced time-structure and isochore (thickness) maps, collected quantitative fault kinematic data and calculated the amount of extension (β -factor). Our results show that the locations of basin-bounding fault systems were controlled by pre-existing crustal-scale shear zones. Within the basin, Permo-Triassic Rift Phase 1 (RP1) faults mainly developed orthogonal to the E-W extension direction. Rift faults control the locus of syn-RP1 deposition, whilst during the inter-rift stage, areas of clastic wedge progradation are more important in controlling sediment thickness trends. The calculated amount of RP1 extension (β -factor) for the Stord Basin is up to $\beta = 1.55$ ($\pm 10\%$, 55% extension). During the subsequent Middle Jurassic-Early Cretaceous Rift Phase 2 (RP2), however, strain localised to the west along the present axis of the South Viking Graben, with the Stord Basin being almost completely abandoned. Rift axis migration during RP2 is interpreted to be related to changes in lithospheric strength profile, possibly related to the ultraslow extension (<1 mm/year during RP1), the long period of tectonic quiescence (ca. 50 myr) between RP1 and RP2 and possible underplating. Our results highlight the very heterogeneous nature of temporal and lateral strain migration during and between extension phases within a single rift basin.

This is an open access article under the terms of the Creative Commons Attribution License, which permits use, distribution and reproduction in any medium, provided the original work is properly cited.

© 2020 The Authors. *Basin Research* published by International Association of Sedimentologists and European Association of Geoscientists and Engineers and John Wiley & Sons Ltd

KEYWORDS

crustal extension, multirifted basin, Northern North Sea, seismic interpretation, tectonics and sedimentation

1 | INTRODUCTION

In multiphase rifts the location of maximum extension (the rift axis) often differs between rift phases. Using numerical forward modelling, several factors have been proposed to control rift axis migration and rift basin abandonment during later extension phases, such as variations in lithospheric and asthenospheric rheology, crustal strength profiles during extension, duration of tectonic quiescence between rift phases (interrift period), and crustal extension rate (Bertotti et al., 1997; Braun, 1992; Naliboff & Buiter, 2015; Tetreault & Buiter, 2018; Tett & Sawyer, 1996; van Wijk & Cloetingh, 2002). Multiphase rifts are common and exist in Thailand (Morley, 2017), the North Falkland Basin (Brandsen et al., 1999), East Greenland (Rotevatn et al., 2018), the northern North Sea (Badley et al., 1984; Færseth, 1996; Gabrielsen et al., 1990; Ziegler, 1992), the Mid-Norwegian margin (Lundin & Doré, 1997; Reemst & Cloetingh, 2000), and the East African Rift (Castaing, 1991; Kolawole et al., 2018; Morley et al., 1990). However, how strain has migrated during and between rift episodes is not well-known for all of these rifts as dense subsurface data coverage is required to image and reconstruct basin structure and the timing of deformation events. Data availability and the well-known geological history of the northern North Sea presents a unique opportunity to study the main controls on rift axis migration between different phases of extension.

The northern North Sea rift developed as a result of two main episodes of crustal extension: a Middle Permian-Early Triassic phase (RP1) and a Middle to Late Jurassic-Early Cretaceous phase (RP2, Figure 1). The rift developed in rheologically and structurally heterogeneous crust, containing a range of structures inherited from the Caledonian collisional orogeny and a subsequent extensional collapse in the Devonian (Fossen, 1992; Osmundsen & Andersen, 1994; Séranne & Séguret, 1987). The ~450 km long, NE-trending, Viking-Sogn graben system roughly defines the RP2 rift axis (Figure 1), whereas RP1 extension was somewhat more distributed across the rift (Badley et al., 1988; Claringbould et al., 2017; Færseth, 1996; Lervik, 2006; Odinsen et al., 2000; Steel, 1993; Steel & Ryseth, 1990; Tomasso et al., 2008). The amount of crustal extension (β -factor) during RP2 is thought to be less than RP1 and mainly accommodated by large normal faults bounding the Viking and Sogn grabens (Bell et al., 2014; Odinsen, et al., 2000; Roberts et al., 1993, 1995). The main RP1 axis and related rift basins are located along the Horda Platform and East Shetland Basin on the east and west of the Viking Graben, respectively (Færseth, 1996; Lervik, 2006; Steel, 1993). Despite

Highlights

- Stord Basin located in the SE northern North Sea developed during Permo-Triassic rifting with $\beta = 1.55 (\pm 10\%)$.
- During the Middle Jurassic-Early Cretaceous rifting Stord Basin is abandoned with $\beta = 1.01 (\pm 10\%)$.
- The rift axis migrates westward from the Stord Basin to the Viking graben during the second rifting event.
- The location of basin-bounding fault systems was controlled by pre-existing crustal-scale shear zones.
- Within the basin, rift faults are developed orthogonal to the Permo-Triassic E-W extension direction.

an improved understanding of RP1 development in the East Shetland Basin and northern Horda Platform, principally due to the availability of large, higher-quality, 3D seismic reflection datasets (Bell et al., 2014; Claringbould et al., 2017; Deng, et al., 2017; Duffy et al., 2015; Tomasso et al., 2008; Whipp et al., 2014), our knowledge of the development and architecture of the Stord Basin, the main RP1 basin in the northern North Sea, is very limited.

Here we use high-quality 2D seismic reflection data and 23 exploration wells to investigate temporal and spatial variations in structural styles and depositional patterns within the Stord Basin during RP1 and RP2 (Figure 1). We also calculate the ratio between cumulative fault displacement and fault length to understand if the RP2 faults are under-displaced relative to RP1 faults, a characteristic thought to be at least partly diagnostic of faults formed from the reactivation of older structures (Deng et al., 2017; Kim & Sanderson, 2005; Paton, 2006; Schultz et al., 2008). We compare our observations on fault displacement versus fault length to scaling relationships identified in the global dataset, using this as a basis to discuss the potential influence of structural inheritance on rift fault and basin geometry. We calculate extension (β -factor) along two profiles across the Stord Basin during RP1 and RP2 and compare them with estimates from other basins in the northern North Sea rift.

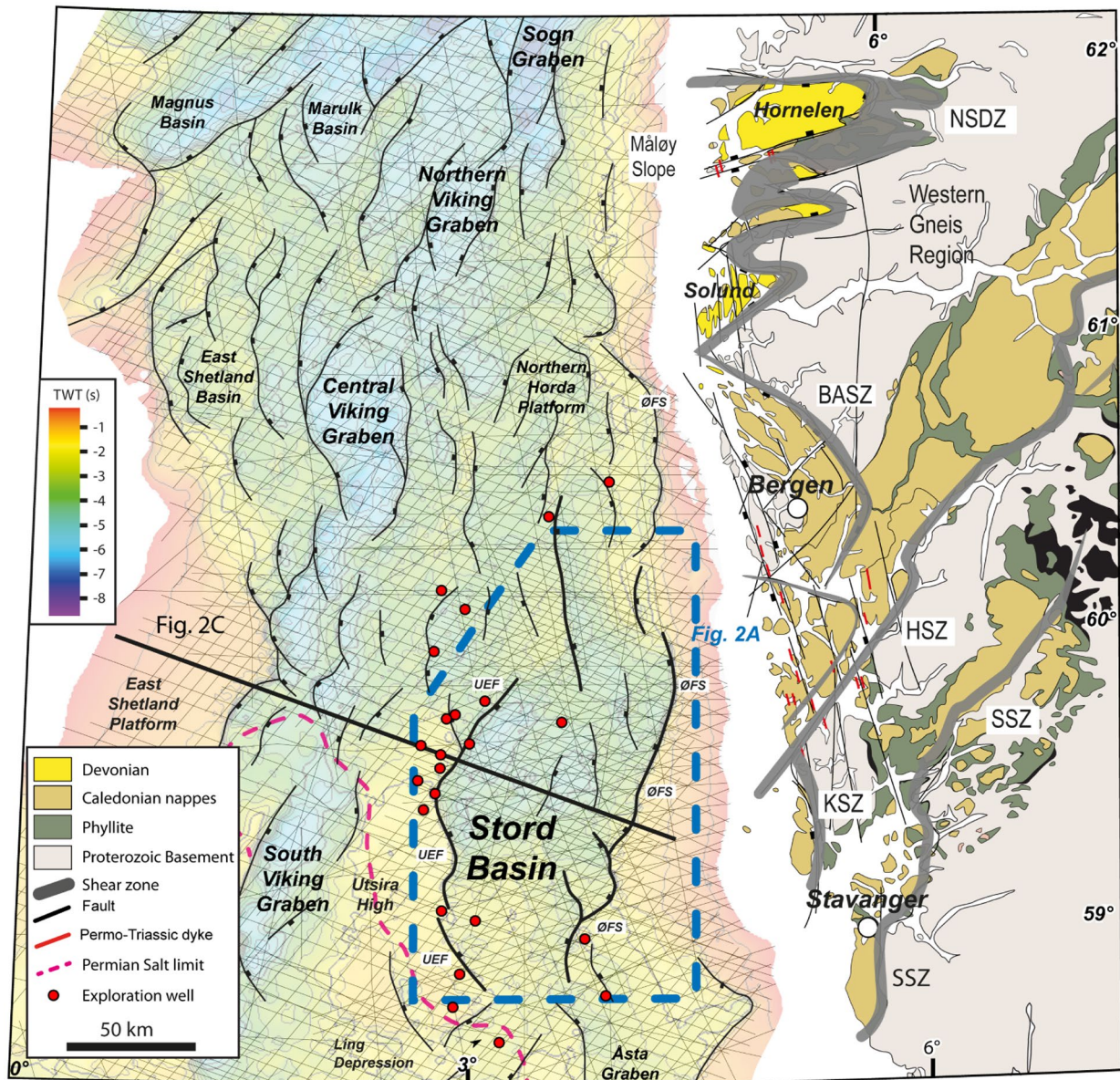


FIGURE 1 Location of the Stord Basin in the northern North Sea, offshore southern Norway shown by blue dashed line. Time-structure map of Base Rift (Base RP1) shows the general structural configuration in the northern North Sea. Thin black lines in the background show 2D seismic profiles utilised in this study. Red dots are exploration wells used for well-seismic tie and stratigraphic correlation

We ultimately compare our observations from the Stord Basin with other multiphase rifts and the predictions of numerical forward models; this provides a basis for discussing the possible reasons for the observed intra-rift strain migration and the ultimate abandonment of the Stord Basin, despite it being the most extended area in the northern North Sea region during RP1. Our results show that the locations of basin-bounding fault systems were controlled by pre-existing crustal-scale shear zones. Within the basin, Permo-Triassic Rift Phase 1 (RP1) faults mainly developed orthogonal to the E-W extension direction. Rift faults control the locus of syn-RP1 deposition, whilst during the inter-rift

stage, areas of clastic wedge progradation are more important in controlling sediment thickness trends. The calculated amount of RP1 extension (β -factor) for the Stord Basin is up to $\beta = 1.55 (\pm 10\%, 55\% \text{ extension})$. During the subsequent Middle Jurassic-Early Cretaceous Rift Phase 2 (RP2), however, strain localised to the west along the present axis of the South Viking Graben, with the Stord Basin being almost completely abandoned. Rift axis migration during RP2 is interpreted to be related to changes in lithospheric strength profile, possibly related to the ultraslow extension ($< 1 \text{ mm/year}$ during RP1), the long period of tectonic quiescence (ca. 50 myr) between RP1 and RP2 and possible underplating.

2 | Geological setting of the northern North Sea

The northern North Sea rift basin developed as a result of Middle Permian–Early Triassic extension followed by thermal cooling and subsidence (RP1) and a Mid–Jurassic to Early Cretaceous extensional phase (RP2) followed by Cretaceous and Cenozoic post-rift thermal subsidence (Badley et al., 1984, 1988; Færseth, 1996; Gabrielsen et al., 1990; Lervik, 2006; Odinsen, et al., 2000; Underhill & Partington, 1993; Ziegler, 1990). Pre-rift crystalline basement in the northern North Sea basin comprises Palaeozoic and older rocks that underwent Caledonian orogenic deformation, followed by extensive crustal stretching in the Devonian. The Caledonian basal thrust zone (*décollement*) was reactivated as a low-angle extensional shear zone during the Devonian post-orogenic extension (Mode I extension, Fossen, 1992). In addition, several major extensional shear zones (Nordfjord–Sogn Detachment Zone, and the Bergen Arc, Hardangerfjord, Karmøy and Stavanger shear zones; Figure 1) developed during this period of Devonian extension (Fossen, 1992; Osmundsen & Andersen, 1994; Séranne & Séguret, 1987; Vetti & Fossen, 2012). These pre-rift structures created a structurally and rheologically heterogeneous crust that was subsequently stretched. Caledonian and post-Caledonian (Devonian) structures were reactivated several times onshore (Fossen et al., 2016; Ksiensyk et al., 2016) and offshore (Fazlikhani et al., 2017; Lenhart et al., 2019; Osagiede et al., 2019; Phillips et al., 2016; Reeve et al., 2014) West Norway. The Carboniferous and Permian strata in the North Sea region is marked by the deposition of post-Variscan clastics of the Rotliegend Group and evaporites of the Zechstein Supergroup, the latter being thickest in the southern North Sea (Heeremans & Faleide, 2004; Ziegler, 1992). These evaporites extend northward into the South Viking Graben and pinch out immediately south of the Stord Basin (Figure 1).

A major rift phase (RP1) in the northern North Sea was driven by E–W extension that started in the Middle Permian and continued into the Early Upper Triassic (ca. 260–220 Ma). The timing of RP1 rifting is based on (a) K/Ar and Ar⁴⁰–Ar³⁹ dating of amphiboles and whole-rock samples from onshore southern Norway dykes, (b) the palaeomagnetic age of fault reactivation of the Nordfjord–Sogn detachment farther north, (c) seismic-stratigraphic interpretation of syn- and post-rift megasequences and (d) palynological dating of Lower Triassic shales in northern Horda Platform (Færseth et al., 1976, 1995; Fossen & Dunlap, 1999; Steel & Ryseth, 1990; Torsvik et al., 1992). The precise timing of RP1 activity is not known, since the Permian–Triassic boundary has not been penetrated by wells or dated across large parts of the northern North Sea basin. In the South Viking and Åsta grabens and the Ling Depression, where pre-RP1 units are

penetrated, RP1-related rocks overlie Zechstein Supergroup evaporites and locally Devonian and Carboniferous sedimentary rocks. At these locations, the top of the Zechstein Supergroup evaporites is defined by a high-amplitude, regionally mappable seismic reflection (Fazlikhani et al., 2017; Jackson & Lewis, 2013; Phillips et al., 2016). Farther north in the northern Horda Platform and East Shetland Basin, Triassic units of various ages locally overlie Caledonian crust and remnants of the Devonian basins. The mapped top of the Zechstein Supergroup and the base Triassic horizon is interpreted as the base RP1 surface (Figure 1).

The deepest RP1 basin in the northern North Sea is the Stord Basin, which is located on the southern Horda Platform (Figure 1). However, RP1 basins are also well-developed in the northern Horda Platform and in the eastern parts of the East Shetland Basin (Claringbould et al., 2017; Odinsen, et al., 2000; Phillips et al., 2019; Steel, 1993; Tomasso et al., 2008). RP1 was followed by post-rift thermal subsidence that lasted from the Early Triassic to Middle Jurassic, and later by Rift Phase 2 (RP2) during the Middle Jurassic to Early Cretaceous (Færseth, 1996; Færseth et al., 1995; Odinsen et al., 2000; Steel & Ryseth, 1990). The amount of extension (β -factor) in the northern North Sea rift varies along and across the rift (Oদিনsen, et al., 2000; Roberts et al., 1993, 1995). RP1 extension is more evenly distributed across the rift compared to RP2, which was focused along the axes of the Viking and Sogn grabens (Badley et al., 1988; Odinsen, et al., 2000; Roberts et al., 1993, 1995; Ter Voorde et al., 2000). RP1 faults have in some cases been reactivated or cross-cut by RP2 faults (Bell et al., 2014; Claringbould et al., 2017; Deng, et al., 2017; Duffy et al., 2015; Tomasso et al., 2008; Whipp et al., 2014). However, in the Stord Basin, despite being located within the relatively well-studied North Sea basin, the magnitude of extension and the distribution of syn-rift depocentres during RP1 and RP2 are poorly constrained.

3 | DATA AND METHODS

3.1 | Data and seismic interpretation

In this study, we use a dense (2–3 km spacing) grid of ~250 regional 2D seismic reflection profiles (NSR-03/12 and SBGS-R94, courtesy of TGS, GNSR-91 and CNST86, courtesy of The Norwegian Petroleum Directorate) and 23 exploration wells in the Stord Basin (Figures 1 and 2a). Seismic reflection profiles have variable orientations and most image to depths of 9-s TWT (two-way time; ~20 to 25 km, Christiansson et al., 2000) providing imaging of the middle and upper continental crust including its uppermost sedimentary layer (Figure 2c). We tied formation tops from exploration wells to the seismic grid using well checkshot data

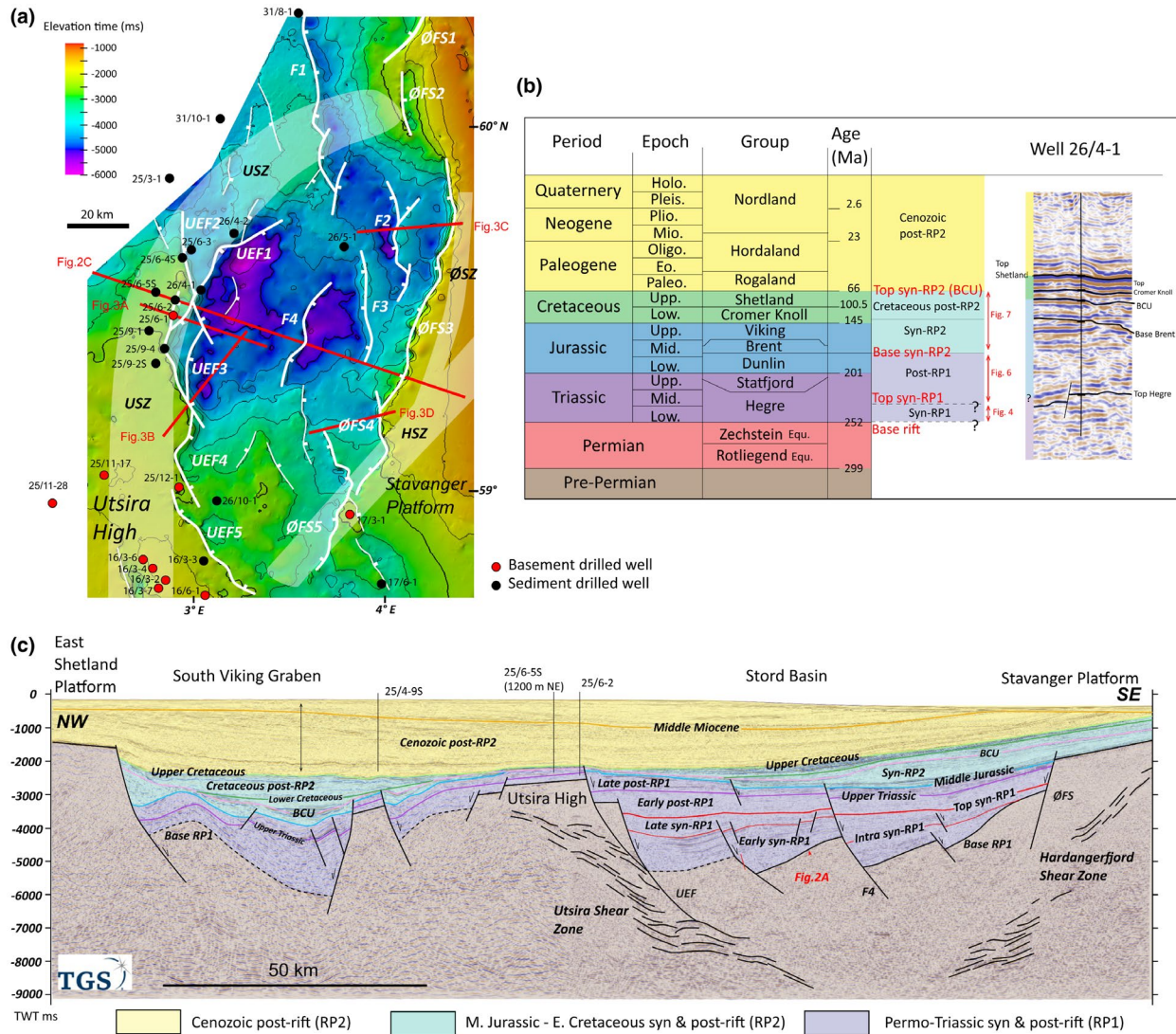


FIGURE 2 (a) Base RP1 time-structure map of the Stord Basin and neighbouring Utsira High to the west and Stavanger Platform to the east. Main basin bounding faults are Øygarden Fault System (ØFS) and Utsira East Fault (UEF), each consisting of several segments. Location of the underlying Caledonian/Devonian Utsira Shear Zone (USZ), Hardangerfjord Shear Zone (HSZ) and Øygarden Shear Zone (ØSZ) are shown, projected to the Base RP1 surface (transparent white polygons). Wells used in seismic well-tie are shown in red (basement drilled) and black. (b) Simplified stratigraphic chart and main interpreted horizons in the Stord Basin. (c) Regional seismic profile (NSR-41153, courtesy of TGS) across the Stord Basin, Utsira High, south Viking Graben and East Shetland Platform. Three main tectono-stratigraphic units are Permo-Triassic (RP1) syn and post-rift, Middle Jurassic - Early Cretaceous (RP2) syn and post-rift covered by Cenozoic to present-day post-rift units

(Figures 2b,c and 3). Eight wells on the Utsira High and in the southeastern part of the study area encounter crystalline basement rocks (Figure 2a). This information is used to identify and map the boundary between the sedimentary cover and crystalline basement. Away from the basement-penetrating wells, our top basement interpretation (Base Rift surface) is defined as a relatively high-amplitude, laterally continuous packages of reflections that separate semi-continuous and sub-parallel reflections defining the sedimentary fill of the northern North Sea and the more chaotic and weaker underlying reflections that characterise the crystalline basement (See

Figure 4 in Fazlikhani et al., 2017 for a detailed description). The oldest mapped seismic horizon penetrated by a borehole defines the top of the Upper Triassic (Top Hegre Group); no wells penetrate the deeper Permian-Triassic boundary in the Stord Basin. However, on the nearby Utsira High, well 25/11-28 encountered a 345 m-thick interval of Permian Rotliegend Group below only 82 m of Triassic Hegre Group rocks. Since the Middle Triassic and older rocks have not been encountered in wells within the study area, seismic horizon interpretations older than the Upper Triassic Top Hegre Group are based on the recognition of major changes in seismic facies and

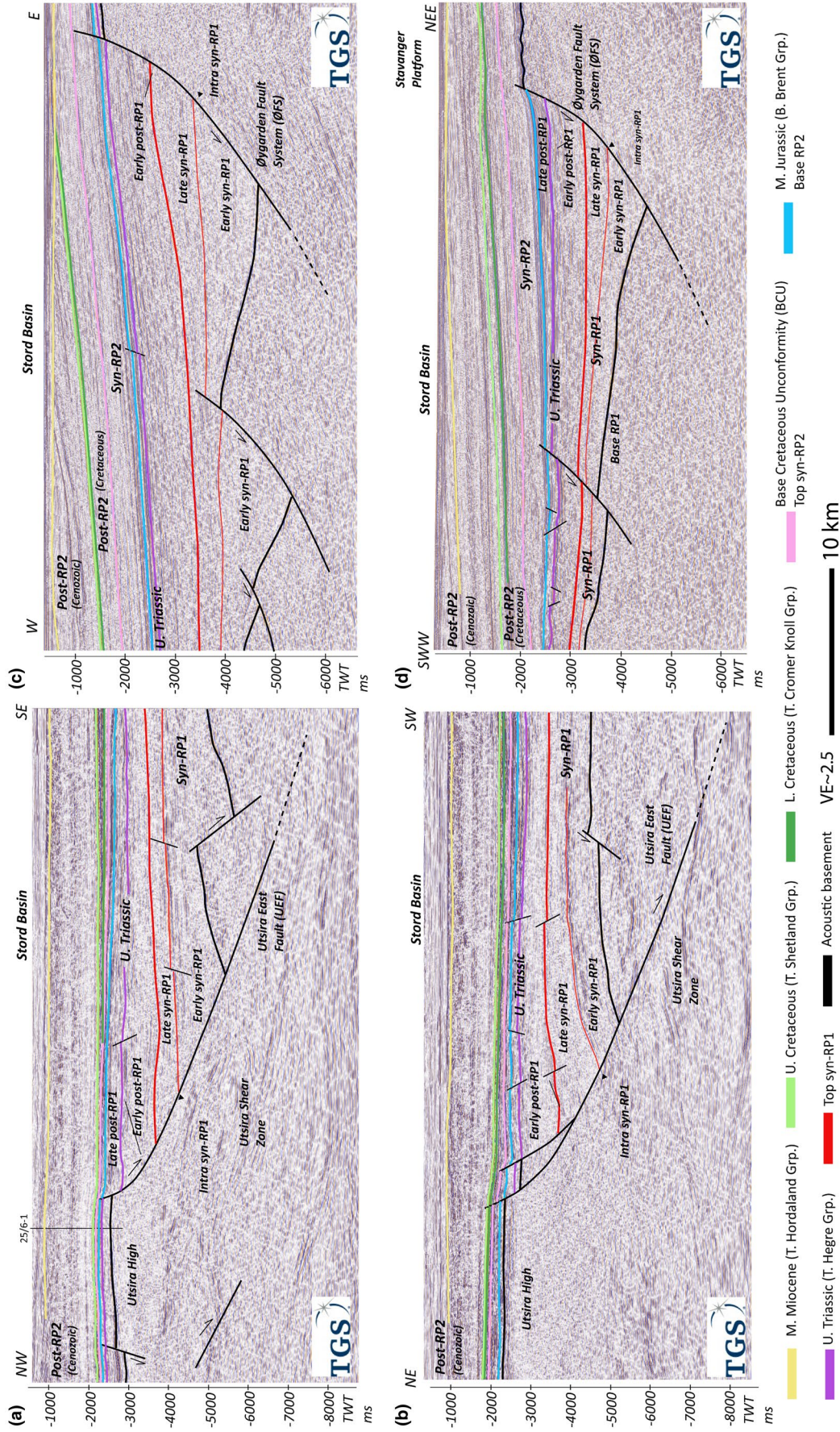


FIGURE 3 Interpreted seismic cross-sections showing seven key horizons above the Base RP1 surface. See Figure 2a for locations. (a) (NSR-11152, courtesy of TGS) and (b) (NSR06-22356, courtesy of TGS) show the western margin of the Stord Basin and the Utsira East Fault (UEF). (c) (SBGS-R94-002, courtesy of TGS) and (d) (GNSR-91-149, courtesy of Norwegian Petroleum Directorate) show eastern margin of the Stord basin and the Øygarden Fault System (ØFS)

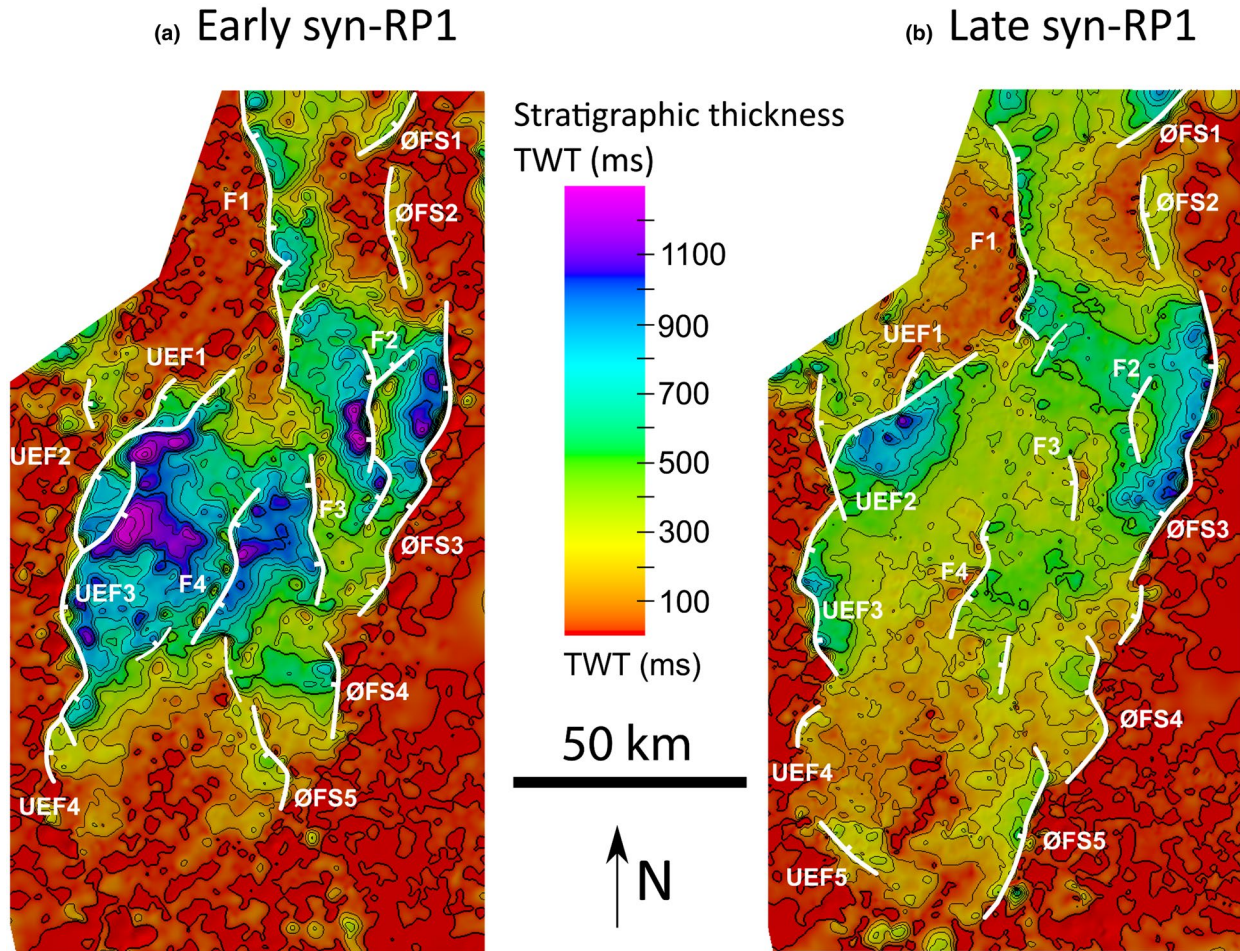


FIGURE 4 Time-thickness maps of (a) early syn-RP1 and (b) late syn-RP1. Highlighted faults show the length of the fault that is active during syn-RP1

reflection terminations. This allows us to divide the interval from Base RP1 to Upper Triassic Top Hegre Group into three seismic units separated by Intra syn-RP1, and Top syn-RP1 horizons (Figures 2c and 3). We mapped five seismic horizons between the top Upper Triassic and the seabed: (a) Early Middle Jurassic (Base Brent Group), marking the Base RP2; (b) Base Cretaceous Unconformity (BCU), marking the transition from syn to post-RP2; (c) Top Lower Cretaceous (Top Cromer Knoll Group), as the top of early Cretaceous post-RP2, (d) Top Upper Cretaceous (Top Shetland Group), top of late Cretaceous post-RP2 and (e) Middle Miocene (Top Hordaland Group, Figures 2 and 3). These horizons thereby bound and thus define pre-, syn and post-RP2 units. Time-thickness maps (isochrons) between key horizons primarily reveal fault-controlled changes in sediment thickness. An absence of fault-related thickness changes defines periods and/or locations of fault inactivity, thus by measuring the lengths of fault-bound, rift-related depocentres, we can define the active, at-surface trace-lengths of the bounding faults (Childs et al., 2003; McLeod et al., 2000; Petersen et al., 1992). The accuracy with which we can measure active fault length and fault throw is

calculated based on the smallest detectable vertical and lateral fault (measured on each time-structure map) offset in millisecond (ms). We applied time-depth relationships obtained from well checkshot data to convert throw values from time to depth (Figure 3 in Fazlikhani et al., 2017 and Appendix S2). We estimate the spatial resolution of our seismic data to be 40 m at 500 ms (TWT) increasing to 60 m at about 5,000 ms (TWT) depth, based on the seismic frequency ranging 20–30 (Hz) and checkshot velocity data.

3.2 | Fault kinematic analysis and rift extension estimation (β -factor)

Fault kinematics analysis is based on the seismically resolvable length of the fault active during a particular time period (the ‘active fault length’) and fault throw and heave measurements. Active fault length is measured for each isochron map where there are thickness changes across the fault (Figures 4 and 5); i.e. the length of the depocentre is used as a proxy for the active fault length. We define and use the active fault lengths to

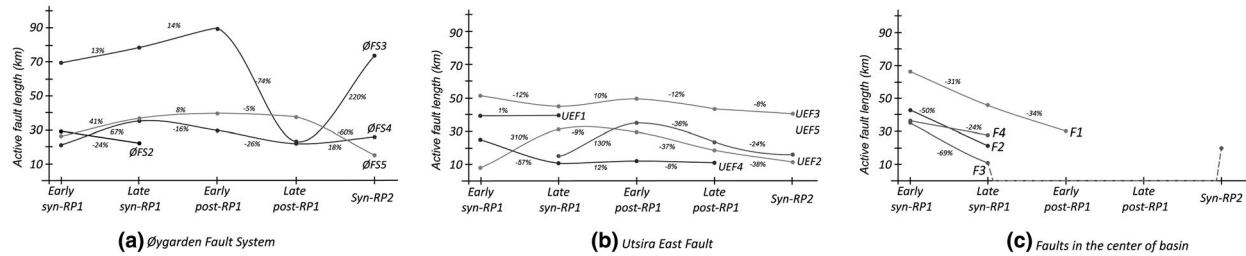


FIGURE 5 Active fault length (km) versus tectonic event plots showing changes in fault length during syn and post-rift events measured on time-thickness maps. Percentages marked on the graphs show the amount of fault expansion or shortening. (a) Active fault length along ØFS segments, (b) Active length of UEF segments and (c) Active fault length plot for the rift faults located in the centre of the Stord Basin. Note that only for ØFS3 and F3 does the active fault length increase significantly during the syn-RP2. Here F3 is reactivated along almost 50% of its initial length and ØFS3 active length increase by 220% in comparison to Late post-RP1

discuss fault lateral propagation and tip retreat during RP1 and RP2, and within the inter-rift periods. Fault throw was constrained by measuring the vertical distance between the hanging wall and footwall cut-offs across the Base RP1 and RP2 seismic horizons. Fault throw data were collected perpendicular to fault strike using the available 2D seismic reflection lines and by creating synthetic sections through time-structure maps where we lacked truly fault-perpendicular 2D seismic lines. Synthetic sections do not contain geophysical data (i.e. a seismic reflection image), but they do show projections of mapped surfaces based on the interpreted 2D seismic grid (Appendix S1).

In the study area, the top acoustic basement is defined as the ‘Base RP1’ and the Base Brent Group (Middle Jurassic) as ‘Base RP2’. Where fault-related folds (drag folds) are observed, the regional surface trend is extrapolated onto the fault surface before throw values were measured to remove the effects of ductile deformation (Long & Imber, 2010). In order to distinguish between fault throw accrued during RP1 and RP2, we subtracted throw values measured across the base RP2 surface from those measured across the base RP1 surface (throw backstripping; e.g. (Veen & Kleinspehn, 2000). In this method, the amount of throw that accumulated on faults during the RP1 and RP2 post-rift stage is included in the throw measurement for both rifting phases. Throw values were first measured in time (ms, TWT) and then depth converted using available velocity-depth information (check-shot data) from exploration wells (Appendix S2). Fault throw data were plotted on throw versus length plots, from which the temporal and spatial development of rift faults were interpreted (see e.g. Jackson & Rotevatn, 2013; Peacock & Sanderson, 1991). It should be noted that when a fault consists of multiple overlapping segments (e.g. UEF3 or F2), we measure the total throw by summing throw for each segment (Appendix S1). Horizontal fault offset (heave) values were also collected and used to estimate the amount of extension (β -factor, McKenzie, 1978) during both rifting phases. We summed backstripped fault heaves (by subtracting RP2 fault heave from RP1 fault heave) across both the Base RP1 and Base RP2 surfaces to calculate pre-rift (T_0) and post-rift (T_1)

length along two transects; this allowed us to estimate total extension (β -factor). By combining time-thickness maps and throw-distance plots, and by estimating the amount of extension, we explore the tectono-stratigraphic development of the Stord Basin.

4 | Structural and stratigraphic framework of the Stord Basin

In the following section, we describe the structural patterns and seismic-stratigraphic units related to RP1 and RP2. The main basin-bounding faults are the Øygarden Fault System (ØFS) to the east and the Utsira East Fault to the west (Figures 1 and 2). The ØFS comprises four segments (ØFS2 – ØFS5) and is c. 200 km long. The northernmost segment (ØFS1) continues northward into the northern Horda Platform and is only partially imaged in the study area (Figure 1, see (Bell et al., 2014). The Utsira East Fault consists of five main segments (UEF1-5) and is c. 100 km long (Figures 1 and 2). For completeness, in this section, we also briefly describe the structure of the pre-Permian basement.

4.1 | Pre-Permian basement (Pre-rift) in the Stord Basin

Caledonian nappe units are drilled offshore on the Stavanger Platform in the southeast portion of the study area and on the Utsira High in the western portion (Fazlikhani et al., 2017; Riber et al., 2015; Slagstad et al., 2011). Towards the southeastern edge of the Utsira High, well 25/12-1 (Figure 2a) drilled through conglomerates and sandstones of possible Devonian age (see Slagstad et al., 2011). The top pre-rift basement (Base Rift horizon) typically appears as a high-amplitude, largely continuous reflection separating mostly continuous and sub-parallel reflections above from chaotic and discontinuous intrabasin reflections below (Figure 3, see Appendix S4 for uninterpreted seismic profiles). These

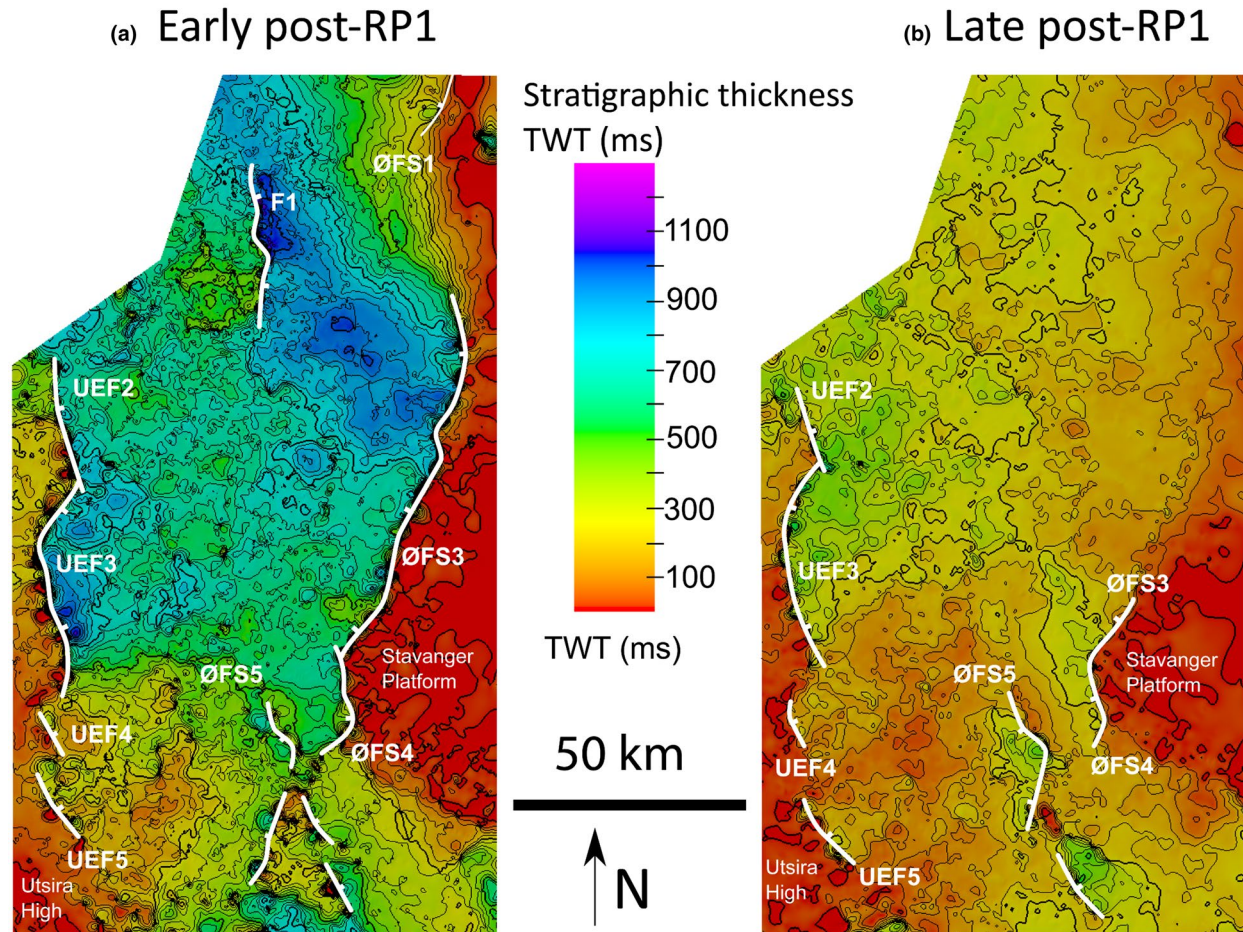


FIGURE 6 Time-thickness maps of (a) early post-RP1 and (b) late post-RP1. Active fault length is shown as white lines. The main early post-RP1 depocentre is located in the hanging wall of ØFS3 and F1 and migrates westward to the hanging wall of UEF2 and UEF3 during the late post-RP1 time

chaotic and discontinuous reflections are interpreted as Caledonian nappes and/or Devonian rocks (seismic facies 2 in Fazlikhani et al., 2017). High-amplitude and dipping reflections below the Base Rift horizon (seismic facies 3 in Fazlikhani et al., 2017) are interpreted as shear zones with normal displacement that developed during the collapse of the Caledonian orogenic lithosphere in the Devonian (Fossen, 1992; Fossen & Hurich, 2005). Two of these shear zones, the Hardangerfjord Shear Zone (HSZ) and Utsira Shear Zone (USZ), bound the Stord Basin to the east and west, respectively (Figure 2a).

4.2 | Permo-Triassic rifting (Rift Phase 1, RP1)

4.2.1 | Syn-RP1

Sedimentary units between the Upper Triassic surface (Top Hegre Group) and Base Rift surface (Figure 3 and Appendix S3) are assigned to the Permo-Triassic rift phase

(RP1, Figure 2b). This unit is subdivided into syn- and post-rift units based on lateral thickness changes observed in seismic reflection data (Figure 2c). Intra syn-RP1 and Top syn-RP1 (Early Triassic?) surfaces divide the syn-RP1 sediments into the 'Early syn-RP1' and 'Late syn-RP1' units (Figures 2b,c and 3).

The early syn-RP1 depocentres are bound by several rift-related faults distributed across the Stord Basin (Figure 4a). In the west, the main depocentres are located in the hanging wall of Utsira East Fault segments 1 and 3 (UEF1 & UEF3, Figure 4a) and are up to 1,500 ms (TWT) thick [up to 4,600 m]. In the centre of the Stord Basin, Faults 4 and 2 (F4 and F2) bound two c. 1,000 ms [TWT, c. 3,400 m] thick depocentres of early syn-RP1 sediments (F2 and F4, Figure 4a). In the east, a depocentre bound to the east by Øygarden Fault System segment 3 (ØFS3) contains up to 1,090 ms [TWT, c. 3,000 m] of early syn-RP1 sediments, whereas this unit thins north-westwards to only 810 ms [TWT, c. 2,300 m] in the hanging wall of Fault 1 (F1, Figure 4a).

Syn-RP1 sequences in the Stord Basin comprise Early Triassic fluvial sandstones (Færseth, 1996; Lervik, 2006;

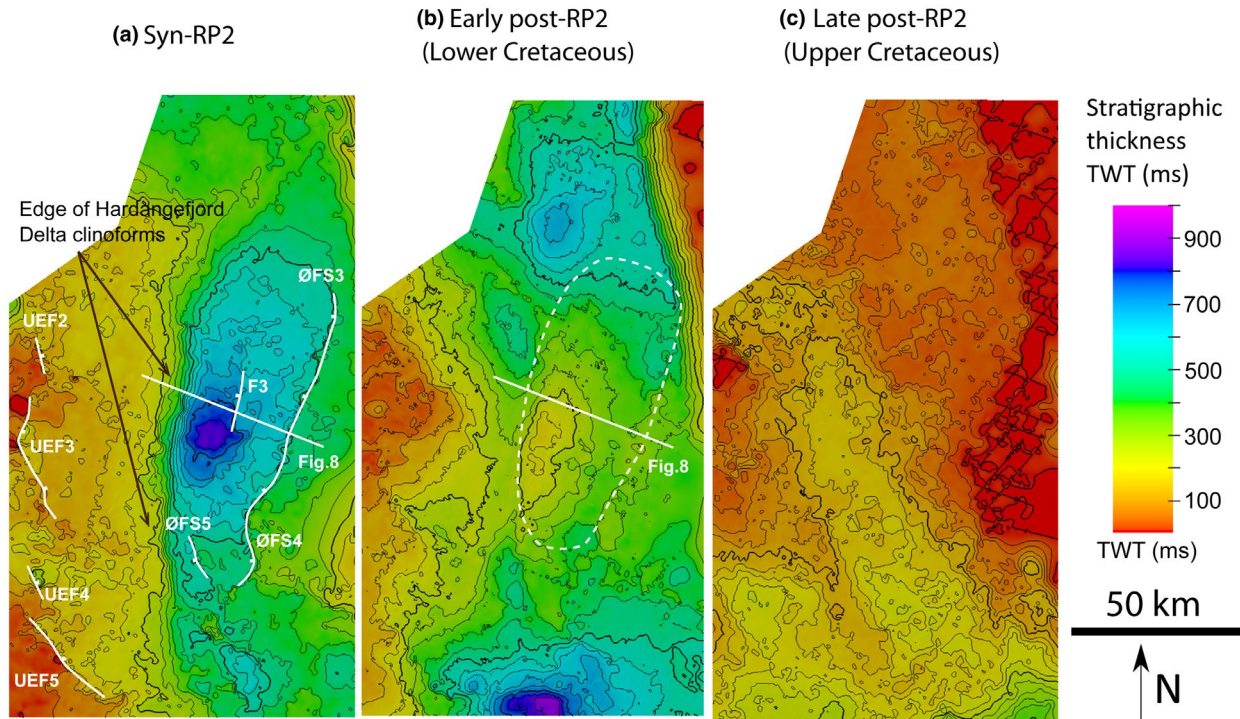


FIGURE 7 Time-thickness maps of RP2. (a) syn-RP2, showing main depocentre and active faults during Middle and Upper Jurassic. (b) lower Cretaceous post-RP2. (c) upper Cretaceous post-RP2. Thickness maximum in the centre of the Stord Basin during syn-RP2 is related to westward propagating Hardangerfjord Delta (see Figure 8). Late Cretaceous post-RP2 is marked by a generally thin and evenly distributed package of sediments in the Stord Basin

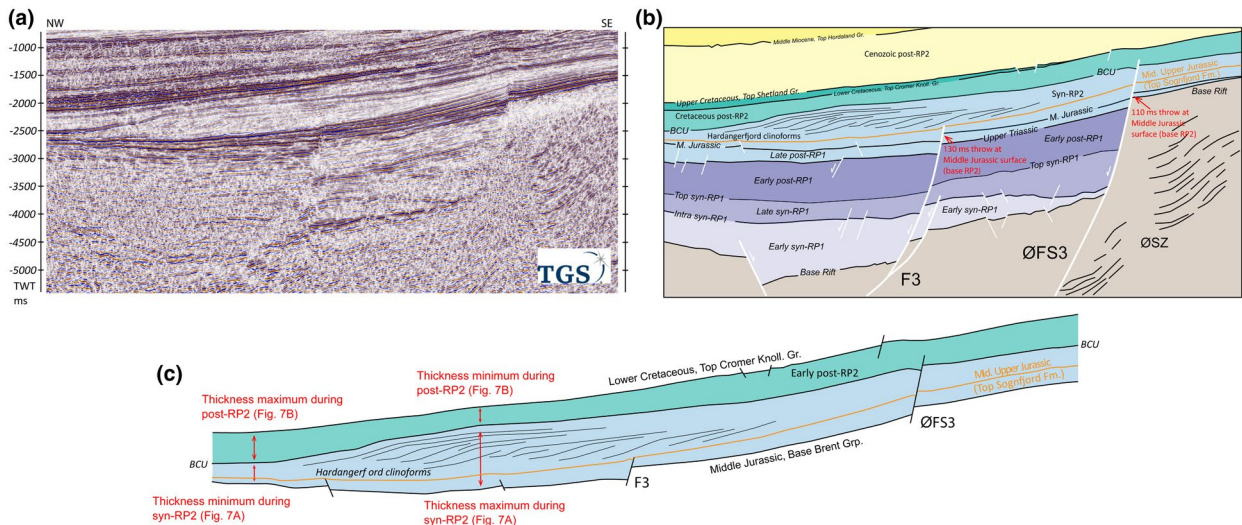


FIGURE 8 (a) Uninterpreted and (b) interpreted section across the eastern Stord Basin showing syn- and post-RP1 and RP2 studied units (courtesy of TGS). RP1 ØFS3 and F3 faults offset the Middle Jurassic surface by 110 ms and 130 ms of throw, respectively. (c) Development of the Hardangerfjord Delta in the Stord Basin synchronous with syn-RP2 fault activities in the northern Horda Platform, Viking Graben and East Shetland Basin. ØSZ = Øygarden Shear Zone

Steel, 1993; Steel & Ryseth, 1990). Since no wells in the Stord Basin have encountered Permian sediments (Rotliegend Group and/or Zechstein Supergroup), it is not possible to differentiate between Permian and early Triassic clastics from seismic reflection data alone. Zechstein Supergroup evaporites were drilled south and west of the Stord Basin in the

Åsta Graben, Ling Depression and Sele and Utsira highs, and the South Viking Graben (Figure 1, see the limit of Zechstein Supergroup). However, on the basement highs west and southeast of Stord Basin, wells 16/3-2, 16/3-4, 16/3-6, 16/6-1, 17/3-1; 25/6-1 and 25/12-1 penetrated basement without encountering any Permian rocks: only wells 16/3-7, 25/11-17

and 25/11-28, located on the Utsira High, drilled through possible Permian clastics (Rotliegend Group) and carbonates (Zechstein Supergroup, Figure 2a).

Away from well constraints, the distinctive signature of evaporites in seismic reflection data (usually low-amplitude, chaotic reflections, contained in strata-discordant bodies (e.g. salt diapirs and pillows) surrounded by higher-amplitude, more continuous seismic reflections) helps us identify the presence of these rocks. However, the presence or absence of Permian clastic rocks in the Stord Basin remains unclear. The absence of Permian rocks in deep wells and apparent lack of Zechstein evaporites as evaluated from seismic reflection data indicate that the Stord Basin was most likely isolated during RP1, disconnected from the Ling Depression and Åsta Graben in the south, and from the South Viking Graben to the west. The apparent lack of early syn-rift deposits south of the Stord Basin (see time-thickness map in Figure 4a) supports this hypothesis. Towards the north, however, the Stord Basin was most likely connected to the northern Horda Platform and north Viking Graben via the hanging wall of F1 (Figure 4a,b).

Major late syn-RP1 depocentres are located in the hanging wall of ØFS3 to the east and UEF1 to the west. In the centre of the Stord Basin, most of the accommodation in the hanging wall of F2, F3 and F4 was filled during early syn-RP1 and the late syn-RP1 sediment thickness is only up to 1 km (in comparison to 3.4 km during early syn-RP1; Figure 4a,b). During late syn-RP1, only the depocentre in the hanging wall of ØFS5 expands laterally (Figure 4b). Major faults that were active during the early syn-RP1 period remained active during late syn-RP1; only UEF5 was newly initiated during the late syn-RP1 (Figure 4a,b). The majority of faults located in the middle, northern and western parts of the basin (F1-4, ØFS2 and UEF3-4) have shorter apparent trace-lengths in late syn-RP2 compared to early syn-RP1; only UEF1 maintained its length, whereas UEF2 is anomalous in that it doubled in length, presumably by lateral tip propagation. In contrast, faults in the eastern Stord basin (ØFS3-5) grew laterally during late syn-RP1, except for ØFS2 in which fault length decreases (Figures 4b and 5).

4.2.2 | Post-RP1

The post-RP1 is defined as the time interval between RP1 and RP2; during this time, the fault activity decreases in comparison to the main RP1 and RP2 rift phases. Post-RP1 is subdivided into 'Early post-RP1' and 'Late post-RP1'. Early post-RP1 is bounded by the Top syn-RP1 (Early Triassic) surface below and Top Hegre Group surface above, whereas the Late post-RP1 is bounded by Top Hegre Group surface below and the Base Brent Group surface above (Figures 2c and 3). During early post-RP1,

three main sediment depocentres are located in the hanging wall of F1, the northern portion of ØFS3 and in the hanging wall of UEF3 (Figure 6a). The early post-RP1 section thins in the southern part of the basin where the interval is only up to 600 m thick in the hanging wall of UEF5 (Figure 6a). Along the ØFS the early post-RP1 section shows significant thickness variations, from 1,900 m in the northern part of ØFS3, thinning by up to 500 m southward. In general, Early post-RP1 sediments (? Early-Middle Triassic to Upper Triassic) are relatively evenly distributed through the basin compared to early and late syn-RP1 (compare Figure 4a,b with Figure 6a); this is related to the cessation of activity on several faults located in the centre of the basin (e.g. F3). Note that NE-dipping faults in the footwall of ØFS5 are outside the study area and are not discussed here (Figure 6a).

During late post-RP1, the key sediment depocentre, which is 700 m thick (c. 500 ms, TWT, in comparison to a 2,200 m thick early post-RP1 depocentre) is located in the hanging wall of UEF2 and UEF3 in the western margin of the basin (Figure 6b). This shows a general westward migration of the main depocentre from Early post-RP1 to Late post-RP1 (Figure 6a,b). Overall, this period is marked by limited thickness variations in the basin in comparison to early post-RP1.

Comparison of Early and Late post-RP1 time-thickness maps show that the active parts of all active faults are shorter during Late post-RP1. In the north and northeast areas, F1 and the majority of ØFS3 are no longer active (Figure 6a,b). In the Early post-RP1, as F2 dies out, the depocentres of F1 and northern ØFS3 merge (Figure 6a). The main fault activity during early post-RP1 occurs along F1 in the north and basin bounding ØFS and UEF faults. During the late post-RP1 main fault activity migrates to the west along the UEF segments (Figure 6a,b). Here it appears that early to late post-RP1 depocentre migration i.e. from the north-northeast to west, is synchronous with the migration of active normal faulting, unlike the diachronous fault activity and rift depocentre migration during syn-RP1 (Figure 6a,b).

4.3 | Middle Jurassic – Early Cretaceous rifting (Rift Phase 2, RP2)

4.3.1 | Syn-RP2

Syn-RP2 units are bounded by the Base Brent Group (Base Middle Jurassic) and the Base Cretaceous Unconformity (BCU) surfaces (Appendix S3). The main depocentre is located in the centre of the basin, where Syn-RP2 is up to 820 ms TWT [c. 1,500 m] thick (Figure 7a). This depocentre is not located in the immediate hanging wall of any fault and is

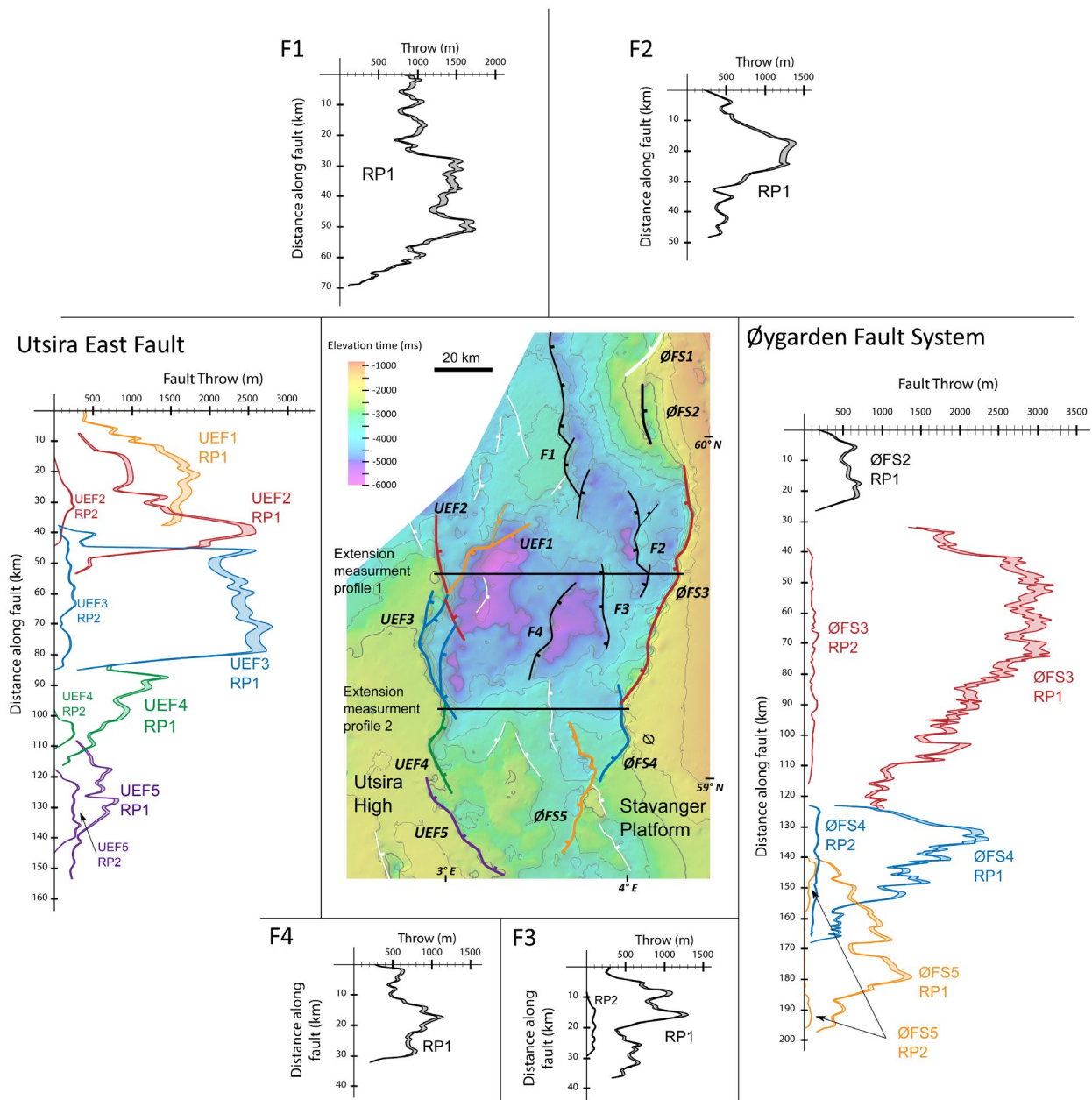


FIGURE 9 Time structure map of Base rift surface in the centre. Along-strike throw values are backstripped and depth converted based on the velocity-depth relationship from checkshot data. Upper and lower curves represent error margins related to the depth conversion. Throw values on the Base RP1 surface show fault activity during RP1 and throw values at Base Middle Jurassic (Base Brent Group) level show fault activity during RP2. Fault throw versus fault length graphs highlights lateral fault throw distribution during RP1 and RP2 in the Stord Basin

associated with a set of westward-prograding clinoforms known as the Hardangerfjord Delta (Gabrielsen et al., 2001; Jarsve et al., 2014; Jarsve, et al., 2014; Sømme et al., 2013). Faults that were active during syn-RP2 are located at the eastern (ØFS3-5 and F3) and western (UEF2-5) basin margins (Figure 7a). ØFS3 was the longest active fault during this period (c. 74 km, Figure 5), yet it accumulated only c. 110 ms (~200 m) of throw in ca. 30 Myr in the Middle Jurassic (Figure 8).

In the central part of the basin, F3 was active during syn-RP2, with an active length of c. 20 km (Figure 7a),

following its last period activity during the Late syn-RP1. The thickest part of Hardangerfjord Delta is located in the hanging wall of F3 (Figure 8). F3 and a relatively small portion of ØFS5 are the only faults reactivated after the ca. 50 myr period of inactivity between Late syn-RP1 (Early Triassic) and syn-RP2 (Middle Jurassic). Reactivation of F3 might be triggered by differential sedimentary loading (Fazlikhani & Back, 2015) associated with westward progradation of the Hardangerfjord Delta. However, a combination of sedimentary loading and crustal extension during syn-RP2 might also

explain the reactivation of F3. The time-thickness map of syn-RP2 (Figure 7a) shows that the Stord Basin was tectonically relatively quiescent during RP2, with only minor fault activity occurring during the very earliest stages of rifting (Figures 7a and 8).

4.3.2 | Post-RP2

The Post-RP2 phase in the Stord Basin spans the Early Cretaceous to the present. The Cretaceous post-RP2 deposits are here subdivided into the Lower and Upper Cretaceous, whereas the Cenozoic post-RP2 is outside the scope of this study and is not discussed further. The Lower Cretaceous sequence is bounded by the BCU below and Top Cromer Knoll Group (top Lower Cretaceous, Appendix S3) above. The main sediment depocentre during this period is located in the northern part of the study area (Figure 7b), reaching a thickness of up to 1,000 m. A thick section also exists at the southern end of the study area (Figure 7b). Sediment deposition, therefore, appears to be directed to underfilled accommodation around the edge of the previously deposited Hardangerfjord Delta (dashed white line in Figure 7b; also see Figure 8c). No fault activity is documented in the Stord Basin during the Early Cretaceous post-RP2 period (Figure 7b). The Upper Cretaceous sequence is marked by an evenly distributed sediment thickness throughout the basin (Figure 7c). In the centre of the basin, the Upper Cretaceous section is only up to 280 m thick, gradually increasing towards the southeast. Like the underlying Lower Cretaceous succession, the Upper Cretaceous succession is virtually unaffected by faulting (Figures 7c and 8).

5 | Fault kinematics

We present a kinematic analysis of basin-bounding faults (Øygarden Fault System, ØFS and Utsira East Fault, UEF) and four significant intra-basin faults (F1-F4) in the Stord Basin are presented below. Throw values in time were measured perpendicular to the fault strike and after depth conversion are throw backstripped revealing the amount of fault throw in meters for RP1 and RP2 (Appendix S3).

5.1 | Øygarden Fault System

The Øygarden Fault System (ØFS) consists of four major segments and bounds the eastern margin of the Stord Basin. ØFS1 extends northwards to the northern Horda Platform beyond the extent of the Stord Basin and it is not, therefore, considered further in this work (see Bell et al., 2014; Whipp et al., 2014). ØFS2 is the only segment that dips to the east and it is not linked to any other segments of the ØFS. This is also reflected in the throw profile measured across the Base RP1 horizon, which shows a maximum throw of 700 m

TABLE 1 Amount of extension (β -factor) measured across the northern and southern Stord Basin during the RP1 and RP2. In order to account for the contribution of subseismic faults 30% is added to the measured values. See the text for details

	Northern Stord Basin		Southern Stord Basin	
	RP1	RP2	RP1	RP2
Profile length, T_1 (km)	83.55	84.30	61.20	61.45
Measured heave	23.30	0.75	11.20	0.25
Initial profile length, T_0 (km)	60.25	83.55	50	61.20
Calculated β	1.39	1.009	1.22	1.004
Corrected for subseismic faulting (+30%)	1.55	1.013	1.32	1.006

close to the centre, decreasing laterally towards the fault tips (Figure 9). ØFS2 was only active during syn-RP1 as shown in time-thickness maps (Figures 4 and 9). Throw along ØFS3 is greatest in the north (c. 3,200 m) and decreases gradually to the south (to c. 1,000 m) where it links with ØFS4 (Figure 9). ØFS3 strikes N-S in the north but rotates NNE-SSW close to its southern tip (Figures 2a and 9). This fault segment was mostly active during RP1, whereas some portions of this fault segment were also active during RP2 (Figures 8a and 9). However, <200 m of throw accumulated on ØFS3 during RP2, only ca. 6% of throw accumulated during RP1 (Figure 9). Nevertheless, the active length of ØFS3 during RP2 was reduced by ca. 18% compared to RP1 (Figure 5a).

ØFS4 is >45 km long, striking N-S in the north and NE-SW in the south (Figure 9). This fault segment accumulated c. 2,300 m of throw during RP1 close to the linkage point with ØFS3, with throw progressively decreasing southwards (Figure 9). During RP2, ØFS4 accumulated c. 200 m of throw, with throw being rather evenly distributed along the structure. Its length shortened slightly during RP2, having reached its maximum length during late syn-RP1 (Figure 5a). Accrued throw during RP2 is <10% of that accumulated during RP1, whereas the fault length was reduced by ca. 25% (Figure 5a).

The 60 km-long ØFS5 segment strikes N-S in the north and NE-SW to the south, with a similar map view geometry to ØFS4 (Figure 9). Maximum throw along ØFS5 is c. 1,400 m, with most of this achieved during RP1 (Figure 9). Unlike ØFS3 and ØFS4, where maximum throw occurs close to their northern tip, the maximum throw on ØFS5 occurs close to its centre. During RP2, two isolated portions of ØFS5 were active; this contrasts with ØFS3 and ØFS4, which were seemingly active along their entire trace-lengths (Figure 9). Throw accumulated on ØFS5 during RP2 reached c. 150 m and c. 100 m in the northern and southern portions of the fault, respectively. The maximum fault length was established during RP1 and this was maintained during the post-RP1 phase. However, fault length decreased to ca. 40% of its original length during syn-RP2 (Figure 5a).

5.2 | Utsira East Fault

UEF1 was only active during syn-RP1 (Figures 4a,b and 5b), during which time it accumulated a maximum throw of c. 1,800 m. UEF2 has a concave-into-the-hanging wall plan-view trace, dips to the east and is c. 45 km long (Figure 9). Throw on this segment increases southwards and reaches a maximum throw of c. 2,600 m close to its southern tip (Figure 9). UEF2 was active throughout syn- and post-RP1, and also syn-RP2, although only ca. 50% of its previously established fault length was reactivated during the latter phase (Figure 9). During RP2, UEF2 accumulated only ca. 10% of the throw accumulated during RP1.

UEF3 is concave-into-the-footwall in map view and consists of at least three east-dipping segments (Figures 2a and 9). This structure is c. 50 km long and accumulated up to 2,800 m of throw during RP1 (Figure 9). During RP1 fault throw was distributed evenly along the structure, with a sharp decrease at the linkage points with neighbouring segments. During RP2, UEF3 only accumulated a further c. 280 m of throw, which is only 10% of that accumulated during RP1. UEF4 is >30 km long, with the northern portion dipping to the ESE and the southern portion to the ENE (Figure 9). Approximately 1,500 m of throw accrued on the northern portion of UEF4 during RP1, close to the linkage point to UEF3. Throw gradually decreases southwards from this point. The maximum fault length established during early syn-RP1 decreased by ca. 60% during Late syn-RP1 and then remained constant (Figure 5b). During RP2, only the southern portion of UEF4 was active, with up to c. 250 m of throw accumulating on a c. 10 km long portion of the fault (Figure 9). UEF5 is c. 35 km long and dips to the northeast (Figure 9). Maximum throw along this fault segment (c. 800 m) occurs near its centre. During RP2, accumulated throw is only ca. 60% of that accrued during RP1, reaching a maximum of 300 m.

5.3 | Intra-basin faults

We focus on four major faults in the centre of the Stord Basin (F1, F2, F3 and F4, Figure 9). These faults have been chosen as they have a significant influence on the internal basin architecture and depositional patterns. Fault 1 (F1) is a segmented fault with an overall eastward dip (Figures 2a and 9), whereas the northern tip of this fault (c. 12 km) extends beyond the study area (Figure 1). Within the study area, F1 is about 70 km long and it was only active during RP1 and early post-rift 1 as evidenced by time-thickness maps, during which time it accumulated a maximum throw of c. 1,700 m (Figures 4, 6a and 9). The fault achieved its near-final length during early syn-RP1, before the active trace-length apparently decreased during late syn-RP1 (Figure 5). The active fault length during early post-RP1 was c. 30 km (Figure 5c).

F2 is located in the hanging wall of ØFS3, strikes N-S, is c. 50 km long, and has an overall westward dip (Figure 9). F2 was active only during syn-RP1 (Figure 4a,b), during which time it accumulated c. 1,400 m of throw near its centre (Figure 9). F3 dips to the east and is c. 37 km long. Maximum throw on F3 during syn-RP1 was c. 1,300 m, decreasing to c. 100 m during syn-RP2. This fault was active during early and late syn-RP1, before being reactivated during syn-RP2 along c. 20 km of the initial fault length established during RP1 (Figures 7a and 9). The maximum syn-RP2 fault throw is only ca. 10% of that accumulated during RP1, with the active part of the fault being ca. 45% shorter during the latter rift phase. Similar fault throw decrease versus fault length shortening pattern during RP2 has also been observed on the ØFS and UEF fault segments. F3 is the only intra-basin fault that was reactivated during RP2, whereas all other faults either die out after RP1 or are continuously active during syn and post-RP1, and onwards into syn-RP2 (Figure 5). F4 is 32 km long and dips broadly south-eastwards (Figure 9). This fault accumulated c. 1,100 m of throw during the RP1 before becoming inactive (Figure 4a,b).

6 | Extension estimate (β factor) across the Stord Basin

The amount of rift-related extension is estimated by summing fault heaves along two E-W profiles across the Stord Basin (see Figure 9 for the location of profiles). We sum horizontal distances between footwall and hanging wall cut-offs across interpreted seismic-scale faults for the Base RP1 and Base RP2 surfaces (top acoustic basement is taken as Base RP1 and Base Middle Jurassic surface as Base RP2). The difference between the present and restored length of the Base RP2 horizon is the extension accumulated during RP2, whereas the difference in length between the restored length of the base RP2 and the present length measured at base RP1 horizon gives the extension occurred during the RP1. An important consideration in measuring crustal extension by heave summation is the contribution of sub-seismic faulting, which is typically estimated to 20%–40% (we present calculated β values in $30\% \pm 10\%$) of the total extension for our level of seismic resolution (Marrett & Allmendinger, 1992; Morley, 1996; Walsh et al., 1991). The resolution relevant here is the lower limit of fault throw detectable from our seismic data, which we estimate to be c. 40 m at 500 ms depth, increasing to c. 60 m at 5,000 ms depth. Another source of error relates to fault block rotation (Sclater & Célérier, 1988) and the amount of erosion on the fault footwall block, particularly on large-displacement, basin-bounding faults such as ØFS and UEF (Morley, 1996). However, only very modest block rotation is observed along the basin-bounding faults in the study area, and fault-bound footwalls appear more or less uneroded. We, therefore, only consider the additional contribution from subseismic faults to be significant.

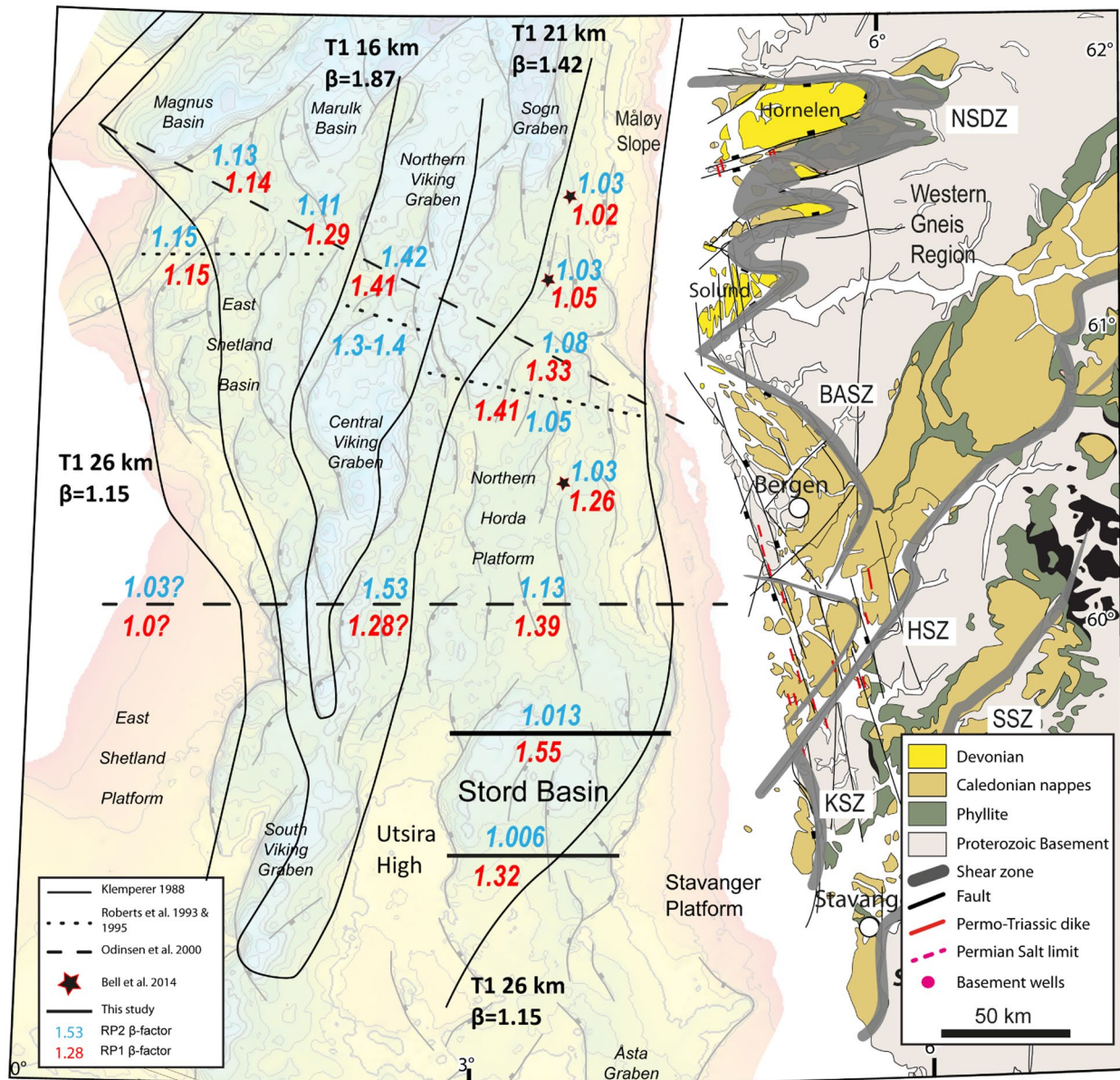


FIGURE 10 Compilation of the calculated amount of extension (β -factor) for RP1 (red values) and RP2 (blue values) in the northern North Sea Basin. β values in the Stord basin are calculated using the fault heave summation method (see text for discussion). Values along the long dashed line (deep seismic section NSDP-1) are calculated using forward modelling with initial crustal thickness $T_0 = 35$ km (Odinsen, et al., 2000). Dotted lines show cross-sections from (Roberts et al., 1995) where β values were calculated using backstripping and reversed modelling (note that the RP2 β values are measured close to the dotted sections of (Roberts et al., 1993)). Post-rift (T_1) crustal thickness $T_1 = 16$, $T_1 = 21$ and $T_1 = 26$ contour lines (continuous black lines) are from Click or tap here to enter text. that are used to calculate β values (for total amount of extension that is not differentiated between rifting phases) in northern North Sea basin. Stars show the values calculated using fault throw estimates by (Bell et al., 2014) in the northern Horda Platform (not corrected for subseismic faulting). Thick black lines are β values estimated in this study

Measured RP1 crustal extension along the two profiles shown in Figure 9 gives a stretching factor (β) of 1.39 (23.3 km of extension) in the north of the basin and $\beta = 1.22$ (11.20 km of extension) in the south (Table 1). Accounting for subseismic faulting ($30\% \pm 10\%$ of total extension) gives $\beta = 1.55$ (33.3 km of extension) and $\beta = 1.32$ (16 km of extension) for the northern and southern areas, respectively. Extension is significantly lower during RP2 than RP1 in

the Stord Basin, with $\beta = 1.009$ (750 m of extension) in the north and $\beta = 1.004$ (230 m of extension) in the south (Table 1). Accounting for subseismic faulting ($30\% \pm 10\%$ of total extension) gives $\beta = 1.013$ (1.07 km of extension) and $\beta = 1.006$ (360 m of extension) for the northern and southern areas, respectively. Comparing the northern and southern parts of the Stord Basin reveals that extension in the north is ca. 52% more than that in the south during RP1 (considering

the $30\% \pm 10\%$ adjustment for sub-seismic deformation) in the north. The RP2 extension in the north is ca. 66% more than that in the south. These results show that the Stord basin mainly developed during RP1, with ca. 95% of total extension (accumulated during RP1, RP2 and inter-rift period) occurring during this time, and that the area experienced a phase of tectonic quiescence during RP2.

7 | DISCUSSION

7.1 | Regional perspectives of crustal stretching

Previous estimates of RP1 and RP2 extension in the northern North Sea have been calculated using several different methods, including crustal-scale thickness and backstripping of lithospheric subsidence. Klemperer, 1988 provides a present-day crustal thickness map for the northern North Sea basin, showing that the crustal thickness along the northern and central Viking Graben is <16 km, and <21 km along the southern Viking Graben (T_1 , post-rift crustal thickness). This value increases towards the eastern and western rift margins to c. 26 km (See Figure 8b in (Klemperer, 1988)). Sources of error for these crustal thickness estimates are related to the depth to Moho, basement velocity, the distribution and the thickness of the Palaeozoic sedimentary section, and the interpretation of the Base Triassic horizon. Assuming a pre-rift crustal thickness (T_0) of 35 km and a simple pure-shear style ductile

deformation of the crust, the total amount of rift-related crustal extension under the north Viking Graben is $\beta = 2.18$, $\beta = 1.66$ and $\beta = 1.34$ for present crustal thicknesses of 16, 21 and 26 km (T_1), respectively (Figure 10). These estimates of crustal stretching are for the complete Late Palaeozoic-Mesozoic rift; RP1 and RP2 are not differentiated.

2D forward modelling that takes into account fault-controlled syn-rift stratigraphy (without including flexural rigidity, (Odinsen, et al., 2000), and post-rift flexural backstripping along two sections on the Horda Platform and on the East Shetland Basin suggest $\beta = 1.4$ for the northern Horda Platform and $\beta = 1.15$ for the East Shetland Basin during RP1 (Figure 10; Roberts et al., 1993, 1995). The same studies estimate $\beta = 1.05$ for the northern Horda Platform, $\beta = 1.3$ – 1.4 for the northern Viking Graben and $\beta = 1.15$ for the East Shetland Basin during RP2. (Odinsen, et al., 2000) applied crustal-scale forward modelling with an initial uniform crustal thickness of 35 km to produce an estimate of $\beta = 1.33$ for RP1 in the northern Horda Platform, $\beta = 1.41$ for the northern Viking Graben, $\beta = 1.29$ for the eastern East Shetland Basin and $\beta = 1.14$ for the western East Shetland Basin (Figure 10). Overall stretching factor estimations by Roberts et al. (1993), Roberts et al. (1995) and Odinsen, et al. (2000)) are in good agreement and slightly higher than the values calculated by fault heave summation by Bell et al., 2014 in the northern Horda Platform and Måløy Slope (Figure 10). Stretching factor estimates for the northern Horda Platform are $<\beta = 1.4$, which is below a proposed minimum value of $\beta = 1.5$ for the initiation of partial melting and

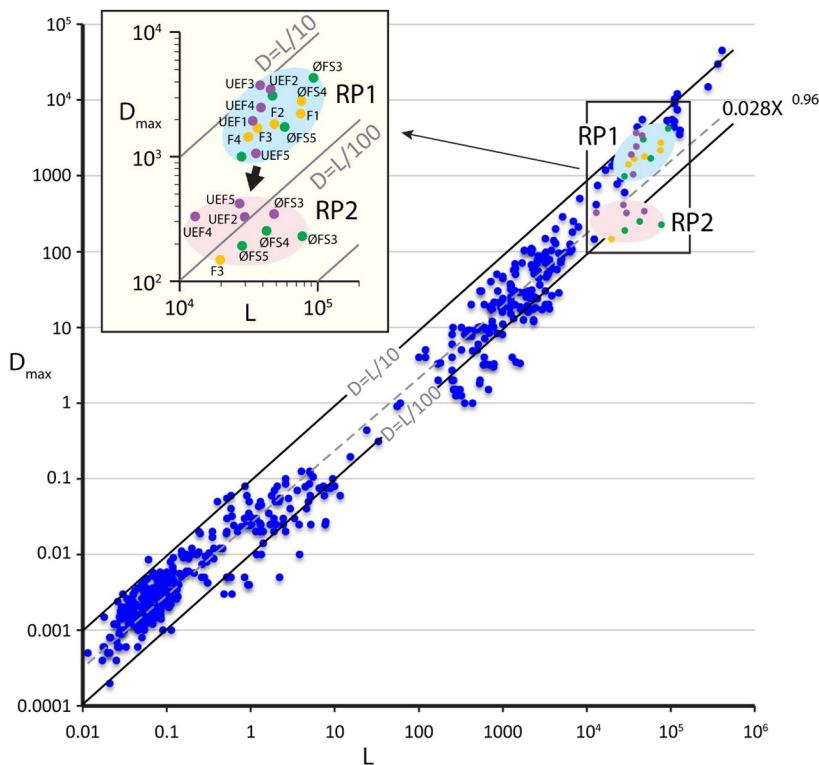


FIGURE 11 Global compilation of fault displacement versus fault length plot (D_{\max}/L , from (Schultz et al., 2008) overlaid by RP1 and RP2 fault displacement and length measurements. Enlarged graph shows fault displacement and length for Øygarden Fault System segments (green circles), Utsira East Fault segments (violet circles) and intra-basin faults (yellow circles) in detail. RP2 faults are under-displaced relative to the fault length, suggesting the reactivation of RP1 faults during RP2

underplating of the crust (Foucher et al., 1982; McKenzie & O'Nions, 1991). However, Wrona et al., 2019 identify potentially large volumes ($472 \pm 161 \text{ km}^3$) of now-crystallised lower crustal melt below this region. In the Oslo Rift and its equivalent offshore Skagerrak Rift, crustal partial melting occurred with crustal stretching estimates of $\beta = 1.4\text{--}1.6$ (Ro & Faleide, 1992).

Considering previous estimates of crustal stretching, our results indicate that in the southern Horda Platform, the Stord Basin experienced larger amounts of extension during RP1 ($\beta = 1.55 \pm 10\%$ in the basin centre) than the northern Horda Platform ($\beta = 1.26\text{--}1.4$). In southern Norway, directly east of the Stord Basin, Permo-Triassic igneous dykes exist (Færseth et al., 1976; Fossen & Dunlap, 1999). The likely presence of magmatic intrusions beneath the northern Horda platform (Wrona et al., 2019), despite the area experiencing less extension during RP1 than the Stord Basin, and the presence of Permo-Triassic dykes onshore southern Norway (c. 50 km east of the Stord Basin) suggest that melting and magmatism might have also occurred in the deeper parts of the Stord Basin, although evidence of magmatic underplating is beyond the resolution of presently available data.

Numerical forward modelling has shown that variations in lithospheric and asthenospheric rheology, varying crustal strength profiles during rifting, length of inter-rift period(s) and overall extension velocity can control rift axis migration and rift basin abandonment (Bertotti et al., 1997; Braun, 1992; Brune et al., 2014; Huisman & Beaumont, 2011; Naliboff & Buiter, 2015; Svartman Dias et al., 2015; Tetreault & Buiter, 2018; Tett & Sawyer, 1996; van Wijk & Cloetingh, 2002). Assuming the Middle Permian – Early Upper Triassic rift phase lasted for ca. 40 million years (ca. 260–220 Ma, Færseth et al., 1976; Færseth et al., 1995; Steel & Ryseth, 1990; Torsvik et al., 1992) and was associated with a stretching factor of $\beta = 1.55 \pm 10\%$ in the Stord Basin (this study), this would correspond to an extension velocity of $<1 \text{ mm/year}$; this is considered ultraslow extension (Pérez-Gussinyé & Reston, 2001; Tetreault & Buiter, 2018; Welford et al., 2010). Numerical modelling by (Tetreault & Buiter, 2018) shows that ultraslow extension results in increased crust-mantle coupling and the creation of symmetric margins. Although crustal extension in the Stord Basin ceased long before continental breakup occurred, the basin is symmetric (Figure 2c). Such a slow extension rate might, therefore, explain the symmetry of the Stord Basin. Numerical models suggest that the rift abandonment will occur either by ultraslow extension rate or by a long period of tectonic quiescence between extension episodes (Naliboff & Buiter, 2015; van Wijk & Cloetingh, 2002). Here, in the Stord Basin, we have a combination of ultraslow extension ($<1 \text{ mm/year}$), possible magmatic underplating modifying crustal strength profile and a long period of tectonic

quiescence (ca. 50 myr) between RP1 and RP2. These factors together may have caused lithospheric hardening, rift basin abandonment and rift axis migration, despite a relatively high amount of extension ($\beta = 1.55 \pm 10\%$) in the Stord Basin during RP1. Similarly, rift basins that developed during the Permo-Triassic, Late Jurassic-Early Cretaceous and Late Cretaceous-Early Tertiary along the mid-Norwegian margin were abandoned as strain migrated overall westward-to-northwestward direction, away from the Norwegian mainland (Gabrielsen et al., 1999; Reemst & Cloetingh, 2000).

7.2 | Influence of preexisting structures on rift fault strike and activity

The Øygarden Fault System (ØFS) bounds the Stord Basin to the east and consists of four main segments in the study area (Figures 1 and 2a). The west-dipping ØFS3 segment strikes N-S over a 30 km extent from its northern tip, which then gradually rotates to an NNE-SSW orientation. This strike rotation of ca. 25° occurs at $N59^\circ33'$, close to the southwestern tip of an onshore section of the Hardangerfjord Shear Zone (HSZ, Figures 1 and 2a). Farther south, ØFS3 strikes subparallel to the offshore extension of the HSZ (Figure 2a, (Fazlikhani et al., 2017). The southern segments, ØFS4 and ØFS5, show an abrupt change in strike of ca. 50° for ØFS4 and 45° for ØFS5 near the offshore extension of the HSZ (Figure 2a). This shear zone, therefore, appears to play a clear role in the development of the ØFS structural style.

Along the western margin of the Stord Basin, the Utsira East Fault (UEF) is aligned with the Utsira Shear Zone (USZ, Figures 1 and 2a). UEF1 strikes NE-SW, parallel to the NE-SW-striking portion of the USZ and both trend oblique to the regional E-W extension direction for RP1 (Færseth et al., 1976, 1995; Steel & Ryseth, 1990; Torsvik et al., 1992). However, UEF2 is not aligned with the USZ trend and instead strikes almost N-S, perpendicular to the regional E-W extension direction (Figure 2a). At this location, the regional stress field related to the E-W extension direction that is localised by the pre-existing USZ, played a key role in controlling rift fault geometry and the development of two fault trends. Further south, UEF3 and UEF4 are aligned with, and most likely, reactivated the USZ. Also here, the variable influence of the pre-existing USZ on the regional E-W extension caused the development of rift faults of variable orientation. In the southwestern edge of the basin, UEF5 strikes NW-SE; it is not, therefore, aligned with the USZ nor perpendicular to the regional stress field. Here other factors, such as lithological differences between the Utsira High (basement high) and sedimentary rocks of southern parts of the Stord Basin, may have promoted strain localisation and controlled the geometry of UEF5 (Bott et al., 1958; Castro et al., 2007; Howell et al., 2019; Phillips et al., 2019).

North of the Stord Basin (at 60° N, Figure 1), the USZ strikes ENE-WSW, sub-parallel to the regional E-W extension direction (Figure 2a). Rift fault F1 strikes overall N-S (Figure 1), although tips of individual fault segments have a more NE-SW strike. F1 developed perpendicular to the E-W regional extension direction; however, rotated segment tips are subparallel to the USZ, most likely associated with mylonitic foliation or layering within the shear zone, both of which may be prone to being preferentially reactivated (Gontijo-Pascutti et al., 2010; Heilman et al., 2019; Kirkpatrick et al., 2013; Morley, 2017; Osagiede et al., 2019; Paton & Underhill, 2004; Salomon et al., 2015). In this case, the orientation of the regional stress field is the primary factor controlling rift fault development, whereas the presence of pre-existing structures locally influences segment tip reorientation.

Within the basin, rift faults (F2, F3 and some minor faults) mainly strike N-S (Figure 2a) and developed perpendicular to the regional E-W extension direction. The exception is F4, which strikes NE-SW, as well as some segments of F1 and F2 (Figure 2a). This may be due to the rotation of the local stress by pre-rift basement structures parallel to the HSZ trend that is not imaged in the available seismic data.

A logarithmic fault displacement-length plot of the studied RP1 faults (Figure 11) shows that all studied rift faults and fault segments plot between $D = L/10$ and $D = L/100$ lines, whereas RP2 fault segments cluster around $D = L/100$ and towards $D = L/1,000$ lines. Comparing our observation with the global displacement versus length compilation (Schultz et al., 2008) suggests that RP2 faults are under-displaced relative to their length (Figure 11). There is now a wealth of evidence that suggests that faults may present with a low D-L ratio due to rapid fault growth (lengthening) in the early stages of fault development without much displacement accrual (i.e. 'constant-length' fault growth; see e.g. Nicol et al., 2005; Rotevatn et al., 2019); this includes faults growing in crust where there is no evidence for large, pre-existing structures (cf. Meyer et al., 2002; Walsh et al., 2002). Therefore, given that (a) the study area has undergone several deformation phases and (b) the observed low D-L ratios are associated with the later-phase (RP2) faults and not the early-phase (RP1) faults, we suggest that structural inheritance induced lengthening-dominated fault growth behaviours during the second rift stage, leading to the observed 'under-displacement' of the RP2 faults. Faults in the Stord Basin strike N-S, NE-SW and NW-SE (e.g. compare faults on time-structure map in Figure 2a), similar to the trend of pre-existing structures related to the Caledonian and/or post-orogenic Devonian tectonic events. These structures may have locally perturbed the regional stress field and influenced rift fault strike and kinematics in the early stages of fault development (Collanega et al., 2019; Osagiede et al., 2019). Later, as extension continues, and

fault segments grew and linked laterally, rift fault activity focuses on fault segments that strike at a high-angle (e.g. N-S) to the E-W regional stress field.

7.3 | Permo-Triassic (RP1) and Middle Jurassic-Lower Cretaceous (RP2) rifting in the Stord Basin and northern North Sea

Slip on RP1 faults in the Stord Basin created significant accommodation for syn-rift sediments to accumulate (Figure 4a,b). The thickest early syn-RP1 depocentres are distributed across the basin, (Figure 4a), which contrasts with the late syn-RP1 phase depocentres that localise next to the basin-bounding UEF and ØFS faults (Figure 4b). The earliest stages of RP1 are, therefore, characterised by distributed faulting and associated depocentres. However, as faults continue to grow, the basin-bounding faults develop as the key strain-accommodating structures, storing the thickest sediments in the hanging wall. During early post-RP1, almost the entire Stord Basin accumulates more than 400 ms (c. 300 m) of sediments (Figure 6a). During this phase, all the basin centre rift faults are buried and depocentres only develop adjacent to basin-bounding ØFS and UEF faults. During the late post-RP1, the thickness of sediments is >400 ms, except in the hanging wall of UEF2 and 3 (Figure 6b). This highlights that by the late post-RP1 almost all accommodation created during RP1 was filled (Figure 6b). It appears that select N-S-striking faults preferentially accrue strain during the early post-RP1 stage and therefore focus deposition in these locations. We would expect these fault segments to preferentially slip under an E-W oriented minimum horizontal compressional stress direction, particularly if the extension rate has decreased during the post-rift subsidence phase.

During the Middle Jurassic to Late Cretaceous, the Stord Basin is characterised by relatively little tectonic activity, and sedimentary loading is a key process in creating sediment accommodation. The westward-prograding Hardangerfjord Delta is a significant depositional feature. The Hardangerfjord Delta is most Late Jurassic (Jarsve, et al., 2014) and is not affected by coeval rift faults. The Hardangerfjord Delta does not extend north of 60°N and is separated from the Brent Delta by the Brage Horst and Oseberg Fault Block, near the Lomre Shear Zone (Fazlikhani et al., 2017). Lower Cretaceous deep-marine sediments (Cromer Knoll Group) preferentially fill accommodation north and south of the Hardangerfjord Delta (Figure 7b).

Basin-bounding rift faults in the Stord Basin are active throughout the RP1 syn- and post-rift periods and into RP2, during which times they accrued only up to 250–300 m of throw. In contrast, in the northern Horda Platform, RP1 faults are reactivated during early post-RP2 and developed throws of up to 650–700 m (Bell et al., 2014; Deng, et al., 2017;

Duffy et al., 2015; Whipp et al., 2014). Such diachronous fault activity during RP2 suggests an overall northward migration of strain offshore Norway between rift phases. This is consistent with the slightly higher RP2 β values calculated in the northern Horda Platform compared to the southern Horda Platform (i.e. Stord Basin, Table 1). Farther north, between 61° and 62°N, the Måløy Slope area was only extended during RP2, whereas basins further west, such as the northern Viking Graben and East Shetland Basin, were extended during both rifting phases (Lenhart et al., 2019; Phillips et al., 2019). On the eastern side of the Viking Graben, three distinct areas are identified: (a) 59°–60°N, where highly extended areas during RP1 (i.e. Stord Basin) are almost abandoned during RP2, (b) 60°–61°N, where rift faults in the moderately extended northern Horda Platform reactivate during RP2 and (c) 61°–62°N, where the Måløy slope is mainly extended during RP2.

Within the Stord Basin, fault activity during RP2 was mainly localised along the basin-bounding UEF and ØFS faults. Here, long-lived, easterly dipping UEF fault segments, which dip away from the new RP2 rift axis in the Viking Graben, accommodated Late Jurassic extension. This contrasts with the East Shetland Basin, which defines the opposite side of the RP2 rift-axis, where newly initiated, easterly dipping faults (i.e. towards the rift axis) cross-cut pre-existing, westerly dipping, RP1 structures (Claringbould et al., 2017; Tomasso et al., 2008). Comparing the timing of faulting in the Stord Basin (i.e. southern Horda Platform), northern Horda Platform and East Shetland Basin shows that: a) RP1 faults in the Stord Basin are continuously active during syn- and post-RP1, and during syn-RP2. Instead of new rift faults initiating during RP2, the easterly dipping UEF fault accommodates the majority of RP2 rift-related strain; (b) in the northern Horda Platform, RP1 faults reactivate in late syn-RP2 and early post-RP2 (Bell et al., 2014; Deng, et al., 2017; Duffy et al., 2015; Phillips et al., 2019; Whipp et al., 2014); and (c) RP1 faults in the East Shetland Basin are cross-cut by easterly dipping RP2 faults (Claringbould et al., 2017; Tomasso et al., 2008). Our study, in addition to data from other areas of the northern North Sea, provide an example of the patterns of strain migration and fault initiation and reactivation, that can occur during multiphase continental extension. The rift kinematics documented here may be more broadly applicable to areas formed in response to multiphase extension of strongly heterogeneous crust.

8 | CONCLUSIONS

Seismo-stratigraphic and structural evolution of the Stord Basin, offshore southern Norway documents a rift basin abandonment and rift axis migration occurred in two rift phases.

Numerical models have shown that rift axes could migrate in regions experiencing several rifting events. However, observations from real rift basins are rare. This study presents a natural case where the first rift axis migrates during the second rifting event. We have shown that rift fault activity migrates during and after rift climax and controls main rift depocentres. Our results reflect the general complexity of rift basin evolution and can be applied to other regions experiencing multiple phases of rifting. Our key findings can be summarised as follows:

- The Stord Basin, located in the southern Horda Platform, developed during the Permo-Triassic rifting phase (RP1) with a stretching factor up to $\beta = 1.55 (\pm 10\%)$. The Stord Basin was abandoned during the Late Jurassic-Early Cretaceous rift phase (RP2, $\beta = 1.01 \pm 10\%$) despite being the most extended area in the northern North Sea rift during RP1. This may be due to the ultraslow extension (< 1 mm/year) and the long period of tectonic quiescence (ca. 50 myear) between RP1 and RP2 leading to changes in lithospheric strength profile and possible underplating, which in turn lead to the westward rift relocation to the Viking Graben during RP2.
- The earliest stages of RP1 are characterised by distributed faulting with associated depocentres; however, as faults continue to develop the basin-bounding faults become the key strain-accommodating structures with associated sediment depocentres. Between syn- and post-RP1 strain migrates to the west from the Øygarden Fault System to the Utsira East Fault and migrates southward along the basin.
- The kilometre-scale basin geometry is controlled by (a) E-W extension and (b) the presence of pre-existing Caledonian/Devonian structures, namely the Utsira Shear Zone (USZ) in the west and Hardangerfjord Shear Zone (HSZ) in the east. Smaller-scale pre-rift basement structures might account for fault segment tip reorientation during RP1.
- RP2 fault throw decreases to ca. 10%–20% of that accumulated during RP1, although active fault length is ca. 75%–80% of active fault length during RP1. During RP2, strain migrates overall northwards into the northern Horda Platform. Sedimentation patterns are primarily controlled by basin thermal subsidence during RP2 and key depocentres are associated with, or adjacent to, the Middle to Late Jurassic Hardangerfjord Delta.
- RP1 faults across the northern North Sea reacted differently to RP2 extension: in (a) the Stord Basin RP1 faults are continuously active during syn- and post-RP1 and into syn-RP2. Rift faults in the centre of the basin are only active up to Early post-RP1, (b) northern Horda Platform RP1 faults reactivate during Late syn-RP2 and Early post-RP2 and (c) in the East Shetland Basin, RP1 faults are mainly cross-cut by RP2 faults.

ACKNOWLEDGEMENT

This contribution forms part of the MultiRift Project funded by the Research Council of Norway (PETROMAKS project 215591) and Equinor to the University of Bergen and partners Imperial College, University of Manchester and University of Oslo. Hamed Fazlikhani is funded by the Geothermal Allianz Bavaria (GAB) at the Friedrich Alexander Universität Erlangen-Nürnberg. The seismic data used in this study are publicly available for download via the DISKOS online portal (<https://portal.diskos.cgg.com>). Thanks to TGS and Bent Erlend Kjølhamar for permission to publish the seismic data and to Schlumberger for providing academic licences for the use of Petrel at the University of Bergen and Friedrich Alexander Universität Erlangen-Nürnberg. We would also like to thank the VISTA programme for supporting the professorship of Rob Gawthorpe. All members of the MultiRift project are thanked for the many fruitful discussions throughout the project. Associate editor Craig Magee and reviewers Folarin Kolawole and Conor O'Sullivan are thanked for their constructive and helpful comments. Open access funding enabled and organized by Projekt DEAL. Open access funding enabled and organized by Projekt DEAL.

CONFLICT OF INTEREST

None.

PEER REVIEW

The peer review history for this article is available at <https://publons.com/publon/10.1111/bre.12522>.

DATA AVAILABILITY STATEMENT

The seismic data used in this study are publicly available for download via the DISKOS online portal (<https://portal.diskos.cgg.com>).

ORCID

Hamed Fazlikhani  <https://orcid.org/0000-0002-1585-2236>

Robert L. Gawthorpe  <https://orcid.org/0000-0002-4352-6366>

[org/0000-0002-4352-6366](https://orcid.org/0000-0002-4352-6366)

Christopher A.-L. Jackson  <https://orcid.org/0000-0002-8592-9032>

[org/0000-0002-8592-9032](https://orcid.org/0000-0002-8592-9032)

Atle Rotevatn  <https://orcid.org/0000-0002-8413-3294>

REFERENCES

- Badley, M. E., Egeberg, T., & Nipen, O. (1984). Development of rift basins illustrated by the structural evolution of the Oseberg feature, Block 30/6, offshore Norway. *Journal of the Geological Society*, *141*(4), 639. <https://doi.org/10.1144/gsjgs.141.4.0639>
- Badley, M. E., Price, J. D., Rambech Dahl, C., & Agdestein, T. (1988). The structural evolution of the northern Viking Graben and its bearing upon extensional modes of basin formation. *Journal of the Geological Society*, *145*(3), 455–472. <https://doi.org/10.1144/gsjgs.145.3.0455>
- Bell, R. E., Jackson, C.-A.-L., Whipp, P. S., & Clements, B. (2014). Strain migration during multiphase extension: Observations from the northern North Sea. *Tectonics*, *33*(10), 1936–1963. <https://doi.org/10.1002/2014TC003551>
- Bertotti, G., Ter Voorde, M., Cloetingh, S., & Picotti, V. (1997). Thermomechanical evolution of the South Alpine rifted margin (North Italy): Constraints on the strength of passive continental margins. *Earth and Planetary Science Letters*, *146*(1), 181–193. [https://doi.org/10.1016/S0012-821X\(96\)00214-2](https://doi.org/10.1016/S0012-821X(96)00214-2)
- Bott, M. H. P., Day, A. A., & Masson-Smith, D. (1958). The geological interpretation of gravity and magnetic surveys in Devon and Cornwall. *Philosophical Transactions of the Royal Society of London. Series A: Mathematical, Physical and Engineering Sciences*, *251*(992), 161–191. <https://doi.org/10.1098/rsta.1958.0013>
- Brandsen, P. J. E., Burges, P., Durham, M. J., & Hall, J. G. (1999). Evidence for multi-phase rifting in the North Falklands Basin. *Geological Society, London, Special Publications*, *153*(1), 425. <https://doi.org/10.1144/GSL.SP.1999.153.01.26>
- Braun, J. (1992). Postextensional mantle healing and episodic extension in the Canning Basin. *Journal of Geophysical Research*, *97*(B6), 8927–8936. <https://doi.org/10.1029/92JB00584>
- Brune, S., Heine, C., Pérez-Gussinyé, M., & Sobolev, S. V. (2014). Rift migration explains continental margin asymmetry and crustal hyper-extension. *Nature Communications*, *5*(1), 4014. <https://doi.org/10.1038/ncomms5014>
- Castaing, C. (1991). Post-Pan-African tectonic evolution of South Malawi in relation to the Karroo and recent East African rift systems. *Tectonophysics*, *191*(1), 55–73. [https://doi.org/10.1016/0040-1951\(91\)90232-H](https://doi.org/10.1016/0040-1951(91)90232-H)
- Childs, C., Nicol, A., Walsh, J. J., & Watterson, J. (2003). The growth and propagation of synsedimentary faults. *Journal of Structural Geology*, *25*(4), 633–648. [https://doi.org/10.1016/S0191-8141\(02\)00054-8](https://doi.org/10.1016/S0191-8141(02)00054-8)
- Christiansson, P., Faleide, J. I., & Berge, A. M. (2000). Crustal structure in the northern North Sea: An integrated geophysical study. *Geological Society, London, Special Publications*, *167*(1), 15. <https://doi.org/10.1144/GSL.SP.2000.167.01.02>
- Claringbould, J. S., Bell, R. E., Jackson, C.-A.-L., Gawthorpe, R. L., & Odinsen, T. (2017). Pre-existing normal faults have limited control on the rift geometry of the northern North Sea. *Earth and Planetary Science Letters*, *475*, 190–206. <https://doi.org/10.1016/j.epsl.2017.07.014>
- Collanega, L., Siuda, K., A.-L. Jackson, C., Bell, R. E., Coleman, A. J., Lenhart, A., Magee, C., & Breda, A. (2019). Normal fault growth influenced by basement fabrics: The importance of preferential nucleation from pre-existing structures. *Basin Research*, *31*(4), 659–687. <https://doi.org/10.1111/bre.12327>
- de Castro, D. L., de Oliveira, D. C., Branco, G. C., & Mariano, R. (2007). On the tectonics of the Neocomian Rio do Peixe Rift Basin, NE Brazil: Lessons from gravity, magnetics, and radiometric data. *Journal of South American Earth Sciences*, *24*(2), 184–202. <https://doi.org/10.1016/j.jsames.2007.04.001>
- Deng, C., Fossen, H., Gawthorpe, R. L., Rotevatn, A., Jackson, C.-A.-L., & Fazlikhani, H. (2017). Influence of fault reactivation during multiphase rifting: The Oseberg area, northern North Sea rift. *Marine and Petroleum Geology*, *86*, 1252–1272. <https://doi.org/10.1016/j.marpetgeo.2017.07.025>
- Deng, C., Gawthorpe, R. L., Finch, E., & Fossen, H. (2017). Influence of a pre-existing basement weakness on normal fault growth during oblique extension: Insights from discrete element modeling. *Journal*

- of *Structural Geology*, 105, 44–61. <https://doi.org/10.1016/j.jsg.2017.11.005>
- Duffy, O. B., Bell, R. E., Jackson, C.-A.-L., Gawthorpe, R. L., & Whipp, P. S. (2015). Fault growth and interactions in a multi-phase rift fault network: Horda Platform, Norwegian North Sea. *Journal of Structural Geology*, 80, 99–119. <https://doi.org/10.1016/j.jsg.2015.08.015>
- Færseth, R. B. (1996). Interaction of Permo-Triassic and Jurassic extensional fault-blocks during the development of the northern North Sea. *Journal of the Geological Society*, 153(6), 931. <https://doi.org/10.1144/gsjgs.153.6.0931>
- Færseth, R. B., Gabrielsen, R. H., & Hurich, C. A. (1995). Influence of basement in structuring of the North Sea basin, offshore southwest Norway. *Norwegian Journal of Geology*, 75, 105–119.
- Færseth, R. B., Macintyre, R. M., & Naterstad, J. (1976). Mesozoic alkaline dykes in the Sunnhordland region, western Norway: Ages, geochemistry and regional significance. *Lithos*, 9(4), 331–345. [https://doi.org/10.1016/0024-4937\(76\)90023-2](https://doi.org/10.1016/0024-4937(76)90023-2)
- Fazlikhani, H., & Back, S. (2015). The influence of differential sedimentary loading and compaction on the development of a deltaic rollover. *Marine and Petroleum Geology*, 59, 136–149. <https://doi.org/10.1016/j.marpetgeo.2014.08.005>
- Fazlikhani, H., Fossen, H., Gawthorpe, R. L., Faleide, J. I., & Bell, R. E. (2017). Basement structure and its influence on the structural configuration of the northern North Sea rift. *Tectonics*, 36(6), 1151–1177. <https://doi.org/10.1002/2017TC004514>
- Fossen, H. (1992). The role of extensional tectonics in the Caledonides of south Norway. *Journal of Structural Geology*, 14(8), 1033–1046. [https://doi.org/10.1016/0191-8141\(92\)90034-T](https://doi.org/10.1016/0191-8141(92)90034-T)
- Fossen, H., & Dunlap, W. J. (1999). On the age and tectonic significance of Permo-Triassic dikes in the Bergen-Sunnhordland region, southwestern Norway. *Norsk Geologisk Tidsskrift*, 79(3), 169–178. <https://doi.org/10.1080/002919699433807>
- Fossen, H., Fazlikhani, H., Faleide, J. I., Ksienzyk, A. K., & Dunlap, W. J. (2016). Post-Caledonian extension in the West Norway–northern North Sea region: The role of structural inheritance. *Geological Society, London, Special Publications*, 439(1), 465. <https://doi.org/10.1144/SP439.6>
- Fossen, H., & Hurich, C. A. (2005). The Hardangerfjord Shear Zone in SW Norway and the North Sea: A large-scale low-angle shear zone in the Caledonian crust. *Journal of the Geological Society*, 162(4), 675. <https://doi.org/10.1144/0016-764904-136>
- Foucher, J.-P., Le Pichon, X., & Sibuet, J. C. (1982). The ocean-continent transition in the uniform lithospheric stretching model: role of partial melting in the mantle. *Philosophical Transactions of the Royal Society of London. Series A, Mathematical and Physical Sciences*, 305(1489), 27–43.
- Gabrielsen, R. H., Færseth, R. B., Steel, R. J., Idil, S., & Kløvjan, O. S. (1990). Architectural styles of basin fill in the northern Viking Graben. In *Tectonic evolution of the North Sea Rifts* (pp. 158–179).
- Gabrielsen, R. H., Kyrkjebø, R., Faleide, J. I., Fjeldskaar, W., & Kjennerud, T. (2001). The Cretaceous post-rift basin configuration of the northern North Sea. *Petroleum Geoscience*, 7(2), 137–154. <https://doi.org/10.1144/petgeo.7.2.137>
- Gabrielsen, R. H., Odinsen, T., & Grunnaleite, I. (1999). Structuring of the Northern Viking Graben and the Møre Basin; The influence of basement structural grain, and the particular role of the Møre-Trøndelag Fault Complex. *Marine and Petroleum Geology*, 16(5), 443–465. [https://doi.org/10.1016/S0264-8172\(99\)00006-9](https://doi.org/10.1016/S0264-8172(99)00006-9)
- Gontijo-Pascutti, A., Bezerra, F. H. R., La Terra, E., & Almeida, J. C. H. (2010). Brittle reactivation of mylonitic fabric and the origin of the Cenozoic Rio Santana Graben, southeastern Brazil. *Journal of South American Earth Sciences*, 29(2), 522–536. <https://doi.org/10.1016/j.jsames.2009.06.007>
- Heeremans, M., & Faleide, J. I. (2004). Late Carboniferous-Permian tectonics and magmatic activity in the Skagerrak, Kattegat and the North Sea. *Geological Society, London, Special Publications*, 223(1), 157. <https://doi.org/10.1144/GSL.SP.2004.223.01.07>
- Heilman, E., Kolawole, F., Atekwana, E. A., & Mayle, M. (2019). Controls of basement fabric on the linkage of rift segments. *Tectonics*, 38(4), 1337–1366. <https://doi.org/10.1029/2018TC005362>
- Howell, L., Egan, S., Leslie, G., & Clarke, S. (2019). Structural and geodynamic modelling of the influence of granite bodies during lithospheric extension: Application to the Carboniferous basins of northern England. *Tectonophysics*, 755, 47–63. <https://doi.org/10.1016/j.tecto.2019.02.008>
- Huisman, R., & Beaumont, C. (2011). Depth-dependent extension, two-stage breakup and cratonic underplating at rifted margins. *Nature*, 473(7345), 74–78. <https://doi.org/10.1038/nature09988>
- Jackson, C.-A.-L., & Lewis, M. M. (2013). Physiography of the NE margin of the Permian Salt Basin: New insights from 3D seismic reflection data. *Journal of the Geological Society*, 170(6), 857. <https://doi.org/10.1144/jgs2013-026>
- Jackson, C.-A.-L., & Rotevatn, A. (2013). 3D seismic analysis of the structure and evolution of a salt-influenced normal fault zone: A test of competing fault growth models. *Geol*, 54, 215–234. <https://doi.org/10.1016/j.jsg.2013.06.012>
- Jarsve, E. M., Faleide, J. I. N., Gabrielsen, R. H. Y., & Nystuen, J. P. (2014). Mesozoic and cenozoic basin configurations in the North Sea. Jarsve, E. M., Maast, T. E., Gabrielsen, R. H., Faleide, J. I., Nystuen, J. P., & Sassier, C. (2014). Seismic stratigraphic subdivision of the Triassic succession in the Central North Sea; integrating seismic reflection and well data. *Journal of the Geological Society*, 171(3), 353–374. <https://doi.org/10.1144/jgs2013-056>
- Kim, Y.-S., & Sanderson, D. J. (2005). The relationship between displacement and length of faults: A review. *Earth-Science Reviews*, 68(3), 317–334. <https://doi.org/10.1016/j.earscirev.2004.06.003>
- Kirkpatrick, J. D., Bezerra, F. H. R., Shipton, Z. K., Do Nascimento, A. F., Pytharouli, S. I., Lunn, R. J., & Soden, A. M. (2013). Scale-dependent influence of pre-existing basement shear zones on rift faulting: A case study from NE Brazil. *Journal of the Geological Society*, 170(2), 237. <https://doi.org/10.1144/jgs2012-043>
- Klemperer, S. L. (1988). Crustal thinning and nature of extension in the northern North Sea from deep seismic reflection profiling. *Tectonics*, 7(4), 803–821. <https://doi.org/10.1029/TC007i004p00803>
- Kolawole, F., Atekwana, E. A., Laó-Dávila, D. A., Abdelsalam, M. G., Chindandali, P. R., Salima, J., & Kalindekafé, L. (2018). Active Deformation of Malawi Rift's North Basin Hinge Zone Modulated by Reactivation of Preexisting Precambrian Shear Zone Fabric. *Tectonics*, 37(3), 683–704. <https://doi.org/10.1002/2017TC004628>
- Ksienzyk, A. K., Wemmer, K., Jacobs, J., Fossen, H., Schomberg, A. C., Süßenberger, A. N., Lünsdorf, K., & Bastesen, E. (2016). Post-Caledonian brittle deformation in the Bergen area, West Norway: Results from K-Ar illite fault gouge dating. *Norwegian Journal of Geology*, 96(3), 275–299. <https://doi.org/10.17850/njg96-3-06>
- Lenhart, A., Jackson, C.-A.-L., Bell, R. E., Duffy, O. B., Gawthorpe, R. L., & Fossen, H. (2019). Structural architecture and composition of crystalline basement offshore west Norway. *Lithosphere*, 11(2), 273–293. <https://doi.org/10.1130/L668.1>
- Lervik, K. S. (2006). Triassic lithostratigraphy of the northern North Sea Basin. *Norwegian Journal of Geology*, 86, 93–116.

- Long, J. J., & Imber, J. (2010). Geometrically coherent continuous deformation in the volume surrounding a seismically imaged normal fault-array. *Journal of Structural Geology*, *32*(2), 222–234. <https://doi.org/10.1016/j.jsg.2009.11.009>
- Lundin, E. R., & Doré, A. G. (1997). A tectonic model for the Norwegian passive margin with implications for the NE Atlantic: Early Cretaceous to break-up. *Journal of the Geological Society*, *154*(3), 545. <https://doi.org/10.1144/gsjgs.154.3.0545>
- Marrett, R., & Allmendinger, R. W. (1992). Amount of extension on "small" faults: An example from the Viking graben. *Geology*, *20*(1), 47. [https://doi.org/10.1130/0091-7613\(1992\)020<0047:AOEOSF>2.3.CO;2](https://doi.org/10.1130/0091-7613(1992)020<0047:AOEOSF>2.3.CO;2)
- McKenzie, D. (1978). Some remarks on the development of sedimentary basins. *Earth and Planetary Science Letters*, *40*(1), 25–32. [https://doi.org/10.1016/0012-821X\(78\)90071-7](https://doi.org/10.1016/0012-821X(78)90071-7)
- McKenzie, D. A. N., & O'Nions, R. K. (1991). Partial melt distributions from inversion of rare earth element concentrations. *Petrology*, *32*(5), 1021–1091. <https://doi.org/10.1093/petrology/32.5.1021>
- McLeod, A. E., Dawers, N. H., & Underhill, J. R. (2000). The propagation and linkage of normal faults: Insights from the Strathspey–Brent–Stattfjord fault array, northern North Sea. *Basin Research*, *12*(3–4), 263–284. <https://doi.org/10.1111/j.1365-2117.2000.00124.x>
- Meyer, V., Nicol, A., Childs, C., Walsh, J. J., & Watterson, J. (2002). Progressive localisation of strain during the evolution of a normal fault population. *Journal of Structural Geology*, *24*(8), 1215–1231. [https://doi.org/10.1016/S0191-8141\(01\)00104-3](https://doi.org/10.1016/S0191-8141(01)00104-3)
- Morley, C. K. (1996). Discussion of potential errors in fault heave methods for extension estimates in rifts, with particular reference to fractal fault populations and inherited fabrics. *Geological Society, London, Special Publications*, *99*(1), 117. <https://doi.org/10.1144/GSL.SP.1996.099.01.10>
- Morley, C. K. (2017). The impact of multiple extension events, stress rotation and inherited fabrics on normal fault geometries and evolution in the Cenozoic rift basins of Thailand. *Geological Society, London, Special Publications*, *439*(1), 413. <https://doi.org/10.1144/SP439.3>
- Morley, C. K., Nelson, R. A., Patton, T. L., & Munn, S. G. (1990). Transfer zones in the East African rift system and their relevance to hydrocarbon exploration in rifts. *Bulletin*, *74*(8), 1234–1253. <https://doi.org/10.1306/0C9B2475-1710-11D7-8645000102C1865D>
- Naliboff, J., & Buitter, S. J. H. (2015). Rift reactivation and migration during multiphase extension. *Earth and Planetary Science Letters*, *421*, 58–67. <https://doi.org/10.1016/j.epsl.2015.03.050>
- Nicol, A., Walsh, J., Berryman, K., & Nodder, S. (2005). Growth of a normal fault by the accumulation of slip over millions of years. *Journal of Structural Geology*, *27*(2), 327–342. <https://doi.org/10.1016/j.jsg.2004.09.002>
- Odinsen, T., Christiansson, P., Gabrielsen, R. H., Faleide, J. I., & Berge, A. M. (2000). The geometries and deep structure of the northern North Sea rift system. *Geological Society, London, Special Publications*, *167*(1), 41–57. <https://doi.org/10.1144/GSL.SP.2000.167.01.03>
- Odinsen, T., Reemst, P., van der Beek, P., Faleide, J. I., & Gabrielsen, R. H. (2000). Permo-Triassic and Jurassic extension in the northern North Sea: Results from tectonostratigraphic forward modelling. *Geological Society, London, Special Publications*, *167*(1), 83–103. <https://doi.org/10.1144/GSL.SP.2000.167.01.05>
- Osagiede, E. E., Rotevatn, A., Gawthorpe, R., Kristensen, T. B., Jackson, C.-A.-L., & Marsh, N. (2019). Pre-existing intra-basement shear zones influence growth and geometry of non-colinear normal faults, western Utsira High-Heimdal Terrace, North Sea. *Journal of Structural Geology*, *130*, 103908. <https://doi.org/10.1016/j.jsg.2019.103908>
- Osmundsen, P. T., & Andersen, T. B. (1994). Caledonian compressional and late-orogenic extensional deformation in the Staveneset area, Sunnfjord, Western Norway. *Journal of Structural Geology*, *16*(10), 1385–1401. [https://doi.org/10.1016/0191-8141\(94\)90004-3](https://doi.org/10.1016/0191-8141(94)90004-3)
- Paton, D. A. (2006). Influence of crustal heterogeneity on normal fault dimensions and evolution: Southern South Africa extensional system. *Journal of Structural Geology*, *28*(5), 868–886. <https://doi.org/10.1016/j.jsg.2006.01.006>
- Paton, D. A., & Underhill, J. R. (2004). Role of crustal anisotropy in modifying the structural and sedimentological evolution of extensional basins: The Gamtoos Basin, South Africa. *Basin Research*, *16*(3), 339–359. <https://doi.org/10.1111/j.1365-2117.2004.00237.x>
- Peacock, D. C. P., & Sanderson, D. J. (1991). Displacements, segment linkage and relay ramps in normal fault zones. *Journal of Structural Geology*, *13*(6), 721–733. [https://doi.org/10.1016/0191-8141\(91\)90033-F](https://doi.org/10.1016/0191-8141(91)90033-F)
- Pérez-Gussinyé, M., & Reston, T. J. (2001). Rheological evolution during extension at nonvolcanic rifted margins: Onset of serpentinization and development of detachments leading to continental breakup. *Journal of Geophysical Research*, *106*(B3), 3961–3975. <https://doi.org/10.1029/2000JB900325>
- Petersen, K., Clausen, O. R., & Korstgård, J. A. (1992). Evolution of a salt-related listric growth fault near the d-1 well, block 5605, Danish North Sea: Displacement history and salt kinematics. *Journal of Structural Geology*, *14*(5), 565–577. [https://doi.org/10.1016/0191-8141\(92\)90157-R](https://doi.org/10.1016/0191-8141(92)90157-R)
- Phillips, T. B., Fazlikhani, H., Gawthorpe, R. L., Fossen, H., Jackson, C.-A.-L., Bell, R. E., Faleide, J. I., & Rotevatn, A. (2019). The Influence of Structural Inheritance and Multiphase Extension on Rift Development, the Northern North Sea. *Tectonics*, *38*(12), 4099–4126. <https://doi.org/10.1029/2019TC005756>
- Phillips, T. B., Jackson, C.-A.-L., Bell, R. E., Duffy, O. B., & Fossen, H. (2016). Reactivation of intrabasement structures during rifting: A case study from offshore southern Norway. *Journal of Structural Geology*, *91*, 54–73. <https://doi.org/10.1016/j.jsg.2016.08.008>
- Reemst, P., & Cloetingh, S. (2000). Polyphase rift evolution of the Vøring margin (mid-Norway): Constraints from forward tectonostratigraphic modeling. *Tectonics*, *19*(2), 225–240. <https://doi.org/10.1029/1999TC900025>
- Reeve, M. T., Bell, R. E., & Jackson, C.-A.-L. (2014). Origin and significance of intra-basement seismic reflections offshore western Norway. *Journal of the Geological Society*, *171*(1), 1. <https://doi.org/10.1144/jgs2013-020>
- Riber, L., Dypvik, H., & Sørli, R. (2015). Altered basement rocks on the Utsira High and its surroundings, Norwegian North Sea. *Norwegian Journal of Geology*. <https://doi.org/10.17850/njg95-1-04>
- Ro, H. E., & Faleide, J. I. (1992). A stretching model for the Oslo Rift. *Tectonophysics*, *208*(1), 19–36. [https://doi.org/10.1016/0040-1951\(92\)90334-3](https://doi.org/10.1016/0040-1951(92)90334-3)
- Roberts, A. M., Yielding, G., Kuznir, N. J., Walker, I., & Dorn-lopez, D. (1993). Mesozoic extension in the North Sea: Constraints from flexural backstripping, forward modelling and fault populations. *Geological Society, London, Petroleum Geology Conference Series*, *4*(1), 1123–1136. <https://doi.org/10.1144/0041123>
- Roberts, A. M., Yielding, G., Kuznir, N. J., Walker, I. M., & Dorn-Lopes, D. (1995). Quantitative analysis of Triassic extension in the northern Viking Graben. *Journal of the Geological Society*, *152*(1), 15–26. <https://doi.org/10.1144/gsjgs.152.1.0015>
- Rotevatn, A., Jackson, C.-A.-L., Tvedt, A. B. M., Bell, R. E., & Blækkann, I. (2019). How do normal faults grow? *Journal of*

- Structural Geology*, 125, 174–184. <https://doi.org/10.1016/j.jsg.2018.08.005>
- Rotevatn, A., Kristensen, T. B., Ksienzyk, A. K., Wemmer, K., Henstra, G. A., Midtkandal, I., Grundvåg, S.-A., & Andresen, A. (2018). Structural inheritance and rapid rift-length establishment in a multiphase rift: The East Greenland rift system and its Caledonian orogenic ancestry. *Tectonics*, 37(6), 1858–1875. <https://doi.org/10.1029/2018TC005018>
- Salomon, E., Koehn, D., & Passchier, C. (2015). Brittle reactivation of ductile shear zones in NW Namibia in relation to South Atlantic rifting. *Tectonics*, 34(1), 70–85. <https://doi.org/10.1002/2014TC003728>
- Schultz, R. A., Soliva, R., Fossen, H., Okubo, C. H., & Reeves, D. M. (2008). Dependence of displacement–length scaling relations for fractures and deformation bands on the volumetric changes across them. *Journal of Structural Geology*, 30(11), 1405–1411. <https://doi.org/10.1016/j.jsg.2008.08.001>
- Sclater, J. G., & Célérier, B. (1988). Errors in extension measurements from planar faults observed on seismic reflection lines. *Basin Research*, 1(4), 217–221. <https://doi.org/10.1111/j.1365-2117.1988.tb00017.x>
- Séranne, M., & Séguret, M. (1987). The Devonian basins of western Norway: Tectonics and kinematics of an extending crust. *Geological Society, London, Special Publications*, 28(1), 537. <https://doi.org/10.1144/GSL.SP.1987.028.01.35>
- Slagstad, T., Davidsen, B., & Daly, J. S. (2011). Age and composition of crystalline basement rocks on the Norwegian continental margin: Offshore extension and continuity of the Caledonian–Appalachian orogenic belt. *Journal of the Geological Society*, 168(5), 1167–1185. <https://doi.org/10.1144/0016-76492010-136>
- Sømme, T. O., Martinsen, O. J., & Lunt, I. (2013). Linking offshore stratigraphy to onshore paleotopography: The Late Jurassic–Paleocene evolution of the south Norwegian margin. *Geological Society of America Bulletin*, 125(7–8), 1164–1186. <https://doi.org/10.1130/B30747.1>
- Steel, R. J. (1993). Triassic–Jurassic megasequence stratigraphy in the Northern North Sea: Rift to post-rift evolution. *Petroleum Geology Conference Series*, 4(1), 299. <https://doi.org/10.1144/0040299>
- Steel, R., & Ryseth, A. (1990). The Triassic — early Jurassic succession in the northern North Sea: Megasequence stratigraphy and intra-Triassic tectonics. *Geological Society, London, Special Publications*, 55(1), 139. <https://doi.org/10.1144/GSL.SP.1990.055.01.07>
- Svartman Dias, A. E., Lavier, L. L., & Hayman, N. W. (2015). Conjugate rifted margins width and asymmetry: The interplay between lithospheric strength and thermomechanical processes. *Journal of Geophysical Research: Solid Earth*, 120(12), 8672–8700. <https://doi.org/10.1002/2015JB012074>
- ten Veen, J. H., & Kleinspehn, K. L. (2000). Quantifying the timing and sense of fault dip slip: New application of biostratigraphy and geohistory analysis. *Geology*, 28(5), 471–474. [https://doi.org/10.1130/0091-7613\(2000\)28<471:QTTASO>2.0.CO;2](https://doi.org/10.1130/0091-7613(2000)28<471:QTTASO>2.0.CO;2)
- Ter Voorde, M., Færseth, R. B., Gabrielsen, R. H., & Cloetingh, S. A. P. L. (2000). Repeated lithosphere extension in the northern Viking Graben: A coupled or a decoupled rheology? *Geological Society, London, Special Publications*, 167(1), 59–81. <https://doi.org/10.1144/GSL.SP.2000.167.01.04>
- Tetreault, J. L., & Buitter, S. J. H. (2018). The influence of extension rate and crustal rheology on the evolution of passive margins from rifting to break-up. *Tectonophysics*, 746, 155–172. <https://doi.org/10.1016/j.tecto.2017.08.029>
- Tett, D., & Sawyer, D. (1996). Dynamic models of multiphase continental rifting and their implications for the Newfoundland and Iberia conjugate margins. *Proceedings of the Ocean Drilling Program, Scientific Results*, 149, 635–647. <https://doi.org/10.2973/odp.proc.sr.149.247.1996>
- Tomasso, M., Underhill, J. R., Hodgkinson, R. A., & Young, M. J. (2008). Structural styles and depositional architecture in the Triassic of the Ninian and Alwyn North fields: Implications for basin development and prospectivity in the Northern North Sea. *Marine and Petroleum Geology*, 25(7), 588–605. <https://doi.org/10.1016/j.marpetgeo.2007.11.007>
- Torsvik, T. H., Sturt, B. A., Swensson, E., Andersen, T. B., & Dewey, J. F. (1992). Palaeomagnetic dating of fault rocks: Evidence for Permian and Mesozoic movements and brittle deformation along the extensional Dalsfjord Fault, western Norway. *Geophysical Journal International*, 109(3), 565–580. <https://doi.org/10.1111/j.1365-246X.1992.tb00118.x>
- Underhill, J. R., & Partington, M. A. (1993). Jurassic thermal doming and deflation in the North Sea: Implications of the sequence stratigraphic evidence. *Petroleum Geology Conference Series*, 4(1), 337. <https://doi.org/10.1144/0040337>
- van Wijk, J. W., & Cloetingh, S. A. P. L. (2002). Basin migration caused by slow lithospheric extension. *Earth and Planetary Science Letters*, 198(3), 275–288. [https://doi.org/10.1016/S0012-821X\(02\)00560-5](https://doi.org/10.1016/S0012-821X(02)00560-5)
- Vetti, V. V., & Fossen, H. (2012). Origin of contrasting Devonian supra-detachment basin types in the Scandinavian Caledonides. *Geology*, 40(6), 571–574. <https://doi.org/10.1130/G32512.1>
- Walsh, J. J., Nicol, A., & Childs, C. (2002). An alternative model for the growth of faults. *Journal of Structural Geology*, 24(11), 1669–1675. [https://doi.org/10.1016/S0191-8141\(01\)00165-1](https://doi.org/10.1016/S0191-8141(01)00165-1)
- Walsh, J., Watterson, J., & Yielding, G. (1991). The importance of small-scale faulting in regional extension. *Nature*, 351(6325), 391–393. <https://doi.org/10.1038/351391a0>
- Welford, J. K., Smith, J. A., Hall, J., Deemer, S., Srivastava, S. P., & Sibuet, J.-C. (2010). Structure and rifting evolution of the northern Newfoundland Basin from Erable multichannel seismic reflection profiles across the southeastern margin of Flemish Cap. *Geophysical Journal International*, 180(3), 976–998. <https://doi.org/10.1111/j.1365-246X.2009.04477.x>
- Whipp, P. S., Jackson, C.-A.-L., Gawthorpe, R. L., Dreyer, T., & Quinn, D. (2014). Normal fault array evolution above a reactivated rift fabric; a subsurface example from the northern Horda Platform, Norwegian North Sea. *Basin Research*, 26(4), 523–549. <https://doi.org/10.1111/bre.12050>
- Wrona, T., Magee, C., Fossen, H., Gawthorpe, R. L., Bell, R. E., Jackson, C.-A.-L., & Faleide, J. I. (2019). 3-D seismic images of an extensive igneous sill in the lower crust. *Geology*, 47(8), 729–733. <https://doi.org/10.1130/G46150.1>
- Ziegler, P. A. (1990). Tectonic and palaeogeographic development of the North Sea rift system. In *Tectonic Evolution of North Sea Rifts* (pp. 1–36).
- Ziegler, P. A. (1992). North Sea rift system. *Tectonophysics*, 208(1), 55–75. [https://doi.org/10.1016/0040-1951\(92\)90336-5](https://doi.org/10.1016/0040-1951(92)90336-5)

SUPPORTING INFORMATION

Additional supporting information may be found online in the Supporting Information section.

How to cite this article: Fazlikhani H, Aagotnes SS, Refvem MA, et al. Strain migration during multiphase extension, Stord Basin, northern North Sea rift. *Basin Res.* 2020;00:1–23. <https://doi.org/10.1111/bre.12522>